Tuning ITAM multiplicity on T-cell receptors can control potency and selectivity to ligand density

Authors:

John R. James[1]

Affiliations:

[1]Molecular Immunity Unit, Department of Medicine, University of Cambridge, MRC-LMB, Cambridge, CB2 OQH, UK

Corresponding/Lead Author:

John R. James

Abstract

The T-cell antigen receptor (TCR) recognizes peptides from pathogenic proteins bound in the MHC molecule. To convert this binding event into downstream signaling, the TCR has phosphorylatable intracellular motifs (ITAMs) that act as docking sites for ZAP70, a cytoplasmic tyrosine kinase. Uniquely, the TCR employs 10 ITAMs to transduce pMHC binding to the cell interior. Why this multivalency is required at the mechanistic level remains unclear. Using synthetic, drug-inducible receptor/ligand pairs, we find that greater ITAM multiplicity primarily enhances the efficacy of these engineered receptors, by increasing the efficiency with which ligand binding is converted into an intracellular signal. This manifests as an increase in the fraction of cells that become activated, rather than directly amplifying the intracellular signal and a more synchronous initiation of proximal signaling. Exploiting these findings, we show that the potency and selectivity of chimeric antigen receptors targeted against cancer can be substantially enhanced by modulating the number of encoded ITAMs.

One-sentence summary

The T-cell antigen receptor uses high multiplicity of ITAM signaling motifs to very efficiently transduce ligand binding into intracellular signaling, a mechanism that can be exploited to increase the efficacy of therapeutically relevant CARs targeted against cancers.

Introduction

T cells are an essential cell-type of our adaptive immune system that are capable of distinguishing between healthy, viable cells and those that are infected by pathogens such as bacteria or viruses. To facilitate the T-cell antigen receptor (TCR) being able to interrogate the intracellular state of potentially abnormal cells, there is a continuous process of peptides derived from both host and pathogen proteins being presented at the cell surface, bound within the MHC protein (pMHC). This allows T cells to efficiently scan host cells for 'foreign' peptides and respond accordingly, by either directly killing the cell, or licensing other cells to do so.

On productive ligand binding, TCR triggering (*1*) begins with the LCK-mediated tyrosine phosphorylation of signal motifs on the intracellular tails of the TCR, known as ITAMs. These motifs then act as docking sites for ZAP70, an intracellular tyrosine kinase, so it can be recruited to the TCR. Provided that the TCR remains bound by ligand, ZAP70 becomes activated and continues to phosphorylate proteins such as LAT, which is a signaling scaffold that nucleates many canonical downstream pathways.

The TCR is constructed from eight protein chains: the TCR$\alpha\beta$ heterodimer is responsible for ligand binding while the CD3$\gamma\varepsilon$, CD3$\delta\varepsilon$ and CD3$\zeta\zeta$ dimers are required for intracellular signaling. CD3ζ comprises 3 ITAMs whereas the remaining CD3 chains have one ITAM each, giving a combined total of 10 ITAMs. A long-standing question in T-cell biology is why the TCR has so many of these binding sites, when almost all other immune receptors function effectively with no more than two (*2*)?

Previous studies on answering this question have found that decreased ITAM multiplicity has a significant effect in T-cell development, where fewer ITAMs leads to diminished positive selection and impaired thymocyte lineage commitment (*2*). A similar approach looking at the effect of

ITAMs number on peripheral T-cell responses suggested that signaling 'scaled' linearly with ITAM count, but this only held true for activation-induced cell proliferation; cytokine production was almost invariant to changes in ITAM number (*3*, *4*). For all these in vivo studies, there was very likely significant adaptation of the signaling network in the mouse during thymocyte development (*5*), making it difficult to directly isolate the effect of ITAM multiplicity on T-cell signaling *per se*. For example, the absence of CD3ζ ITAMs does not cause thymic positive selection to fail (*4*, *6*), but rather significantly skews the TCR sequences that undergo selection, suggesting that the genetic perturbation can be well tolerated by thymocyte development, but nonetheless distorts the peripheral T-cell population (*7*). This perhaps explains why no consensus has been reached from these types of experiments on the mechanistic explanation for high TCR ITAM multiplicity. A more recent biophysical study has suggested that increased ITAM number has an effect on TCR potency through an entropic mechanism (*8*), but only looked at phosphorylation of the TCR itself and not any downstream signaling output to show if this effect was propagated through the reaction network.

More generally, in previous experiments only the average signaling response of the population has been correlated with the number of TCR ITAMs, making it difficult to elucidate whether modulating number of ITAMs affects the signaling output level homogeneously in all triggered cells, or the proportion of cells that respond. This information is essential to understand the causative mechanism for ITAM multiplicity in the TCR.

Because of these points, we wanted to directly address the mechanistic effect of receptor ITAM multiplicity without perturbing the underlying signaling network, and to measure the output response at the single-cell level to identify how ITAM modulation was manifested in downstream T-cell activation. We find that increasing the number of ITAMs robustly enhances the efficacy, or probability of signal transduction by synthetic T-cell receptors, and that this primarily drives an

increase in the fraction of activated cells, rather than simply amplifying the downstream response. We then show that these conclusions can be exploited to improve the efficiency of a new class of therapeutics targeted against cancer antigens.

Results

A synthetic, drug-inducible T-cell receptor system

To help elucidate the mechanistic requirement for high receptor ITAM multiplicity on T-cell signaling in a quantitative manner, we needed a means to vary the number of ITAMs in isolation from changes to receptor expression or affinity, and without the overlaid and potentially confounding effects of network adaptation. We therefore designed synthetic receptors that could be expressed in T cells in the presence of the endogenous TCR complex, so that basal signaling in the underlying network would not be disrupted (Fig. 1A). These new receptors utilize an extracellular ligand-binding domain based on the FKBP protein that provides an entirely orthogonal, or independent, T cell input. To create synthetic receptors expressing 0 – 3 ITAMs, we used the extracellular protein domains of CD86, a known monomer (*9*), as a scaffold to link the FKBP domain to the intracellular signaling region of the CD3ζ chain (Fig. 1A). CD3ζ normally encodes 3 ITAMs; to decrease this number, point mutations within the ITAMs of the CD3ζ chain were used to create equivalent receptors with 0, 1 or 2 functional ITAMs. To construct a synthetic receptor that expressed the full complement of 10 ITAMs, we repurposed the endogenously-expressed complete TCR complex by introducing a modified version of the TCRα chain that encoded the FKBP domain extracellularly into T cells (Fig. 1A). Importantly, the binding affinity of these different synthetic receptors is invariant to ITAM number and equivalent surface expression of the receptors could be quantified and controlled for with flow cytometry through an extracellular HA-epitope present on all constructs.

A key feature of the FKBP domain is that its interaction with its binding partner, FRB (*10*), is entirely dependent on the presence of a small-molecule (*11*). Normally this is the drug rapamycin, which can interfere with T-cell activation (*12*). However, expressing FRB with the T2098L mutation permits use of a rapamycin analog (a ‘rapalog’, known as AP21967 or A/C heterodimerizer) that has negligible binding to the equivalent domain of mTOR endogenously

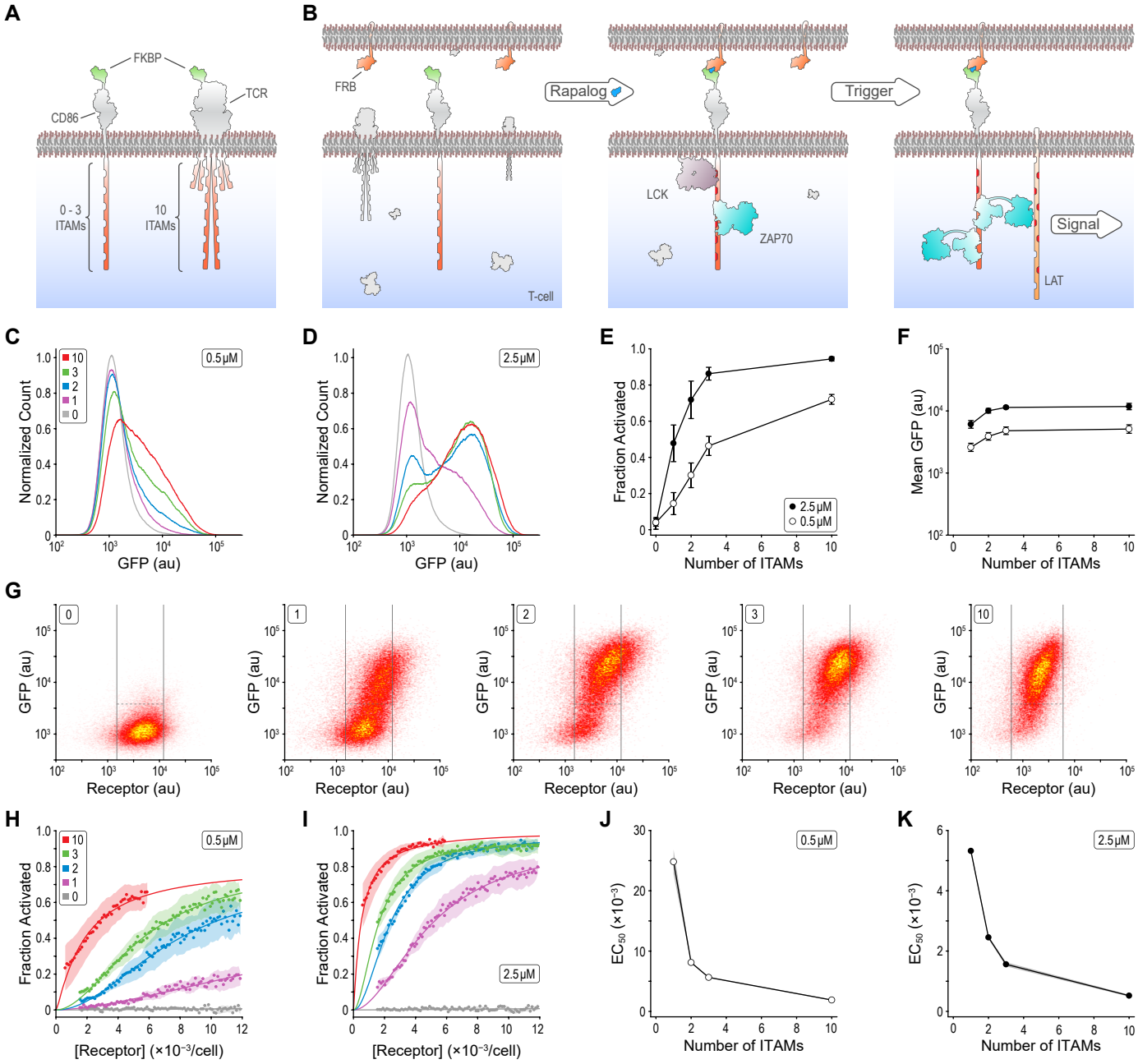

Fig. 1. T-cell signaling potency is enhanced by greater ITAM multiplicity. (**A**) Schematic of the synthetic receptors. For receptors encoding 0-3 ITAMs, the FKBP domain was expressed at the extracellular terminus of CD86 and fused to the intracellular sequence of CD3ζ, with point mutations used to disable the ITAMs when required. For the receptor with 10 ITAMs, the FKBP domain was expressed at the extracellular terminus of the TCRα chain, which was then incorporated into the complete endogenous TCR complex. (**B**) Schematic of synthetic receptor triggering, with proteins approximately to scale. The receptor is expressed in T cells in the presence of endogenous TCR. Conjugation with cells presenting FRB, the cognate FKBP ligand, drives receptor engagement but only in the presence of the rapalog drug (AP21967). This leads to receptor triggering through LCK-mediated phosphorylation of the receptor and the subsequent recruitment of the cytoplasmic kinase ZAP70 and its activation, shown as an 'opening' of the structure, which causes phosphorylation of proteins such as LAT that initiate downstream signaling. (**C** and **D**) Jurkat T cells expressing the synthetic receptor encoding the number of ITAMs shown in legend were activated with FRB-expressing Raji B cells in the presence of 0.5μM (C) or 2.5 μM (D) rapalog. Representative flow cytometry data from one experiment of T cell activation is shown, measured by NFAT-mediated GFP expression, with cells gated for equivalent receptor surface expression. (**E** and **F**) Data from C and D were used to calculate the fraction of T cells that had been activated (E) and the mean GFP intensity of this activated fraction (F) at the rapalog concentration shown in the legend. The mean of three independent experiments is shown for each data point, with error bars representing SEM. (**G**) Density plots of activation-induced GFP expression against synthetic receptor expression with differing ITAM multiplicity (white box). Vertical lines denote the range of receptor expression analyzed and the horizontal dashed line shows the threshold for designating a cell as activated. (**H** and **I**) The fraction of activated Jurkat T cells plotted against receptor expression is shown for all variants of the synthetic receptor in the presence of 0.5μM (H) or 2.5 μM (I) rapalog. Beads with known amounts of fluorophores were used to convert relative fluorescence data from the flow cytometer to absolute surface density. The mean of three independent experiments is shown at each binned expression level, along with a bounding area representing SEM. Datasets are fit using a logistic function. (**J** and **K**) The receptor density required to cause half-maximal cell activation (EC_{50}) was calculated from datasets (H and I) and is shown as a function of the number of ITAMs encoded by the receptor in the presence of 0.5 μM (J) or 2.5 μM (K) rapalog. A 95% confidence interval is shown as a bounding area.

found in T cells. We used Raji B cells that expressed extracellular FRB as the ligand-presenting cell, where engagement between these cells and the synthetic receptor-expressing T cells in the presence of the rapalog can drive receptor triggering and subsequent downstream T-cell activation (Fig. 1B). An important advantage of this drug-inducible receptor system is that it can provide fine temporal control over the initiation of signaling within the physiological context of apposing cell membranes, something that has previously not been possible with other methods for receptor activation. We have also previously shown that a receptor based on FKBP can efficiently recapitulate TCR-mediated triggering (*13*).

ITAM number enhances receptor potency by increasing its efficacy

We hypothesized that there could be two non-exclusive means by which increased ITAM multiplicity could affect T-cell output. This first is that the primary function of multiple ITAMs is to 'amplify' the T-cell input. This would predict that more ITAMs increase the absolute level of a functional readout of activated cells, but would have little effect on the fraction of cells that responded (fig. S1A). An alternative explanation is that having more ITAMs on a receptor enhances its potency, increasing the fraction of bound receptors that are capable of transducing a signal into the cell. This would not increase the absolute level of a cellular output but rather the number of cells that become activated (fig. S1B). Crucially, it would be very difficult to distinguish these mechanistic explanations for ITAM multiplicity when only the average output response of the population is measured (fig. S1B).

To provide the data required to distinguish between these two models and understand the functional effect of ITAM multiplicity, we utilized the synthetic receptors described above to measure downstream T-cell signaling at single-cell resolution with defined levels of signaling input. Jurkat T cells expressing the synthetic receptors with 0 – 3 or 10 ITAMs were conjugated with Raji B cells expressing the cognate FRB domain in the presence of the dimerizing rapalog drug. We used two different concentrations of the rapalog to explore the effect of ITAM multiplicity at different cell

signaling input ‘strengths’. After stimulation of the cells for 16 hours, we measured *de novo* gene expression on activation mediated by the NFAT transcription factor, in a Jurkat T-cell clone that expresses the fluorophore GFP under the control of NFAT-responsive elements. We could therefore measure GFP intensity as a readout of downstream signaling output at the single-cell level (Fig. 1, C and D), and used histogram unmixing to recover the distribution of activated cells from the GFP output histograms (fig. S1C). We found that the number of ITAMs had a substantial impact on the fraction of cells that responded to stimulation (Fig. 1E) but did not greatly affect the overall magnitude of the output response, especially when more than one ITAM was present (Fig. 1F). This held true at both ‘low’ (Fig. 1C) and ‘high’ (Fig. 1D) levels of receptor input mediated by the different rapalog concentrations. We also measured the effect of ITAM multiplicity on IL-2 cytokine secretion using an equivalent assay and found that IL-2 production correlated well with the fraction of activated cells (fig. S2).

As an alternative downstream functional output, we measured activation-induced CD69 expression, which is driven by the AP-1 transcription factor (*14*). We observed the same effects of ITAM multiplicity, with a substantial increase in the fraction of activated cells with essentially no amplification of the absolute levels of CD69 (fig. S1D-G). A recent study has suggested that T cells show increased upregulation of CD69 when presented with increasing ligand density (*15*), something we also observed (fig. S1G), suggesting CD69 is not an entirely digital response. This data also showed that the conjugation efficiency with the B cells was sufficient to activate essentially the entire population of T cells, implying that the signaling threshold for CD69 upregulation was lower than that for the NFAT-GFP reporter where complete activation was not always observed.

By pooling T cells that had been transduced with synthetic receptors driven by promoters of different efficiencies, we could express a wide range of the receptors at the cell surface within a

single experiment. This allowed us to quantitatively determine the relationship between the cellular input and output to the signaling network whilst varying the number of ITAMs (Fig. 1G and fig. S3). For the subsequent analysis, the absolute levels of receptor expression were quantified using beads with known amounts of fluorophores to calibrate the flow cytometer prior to analyzing the samples. Receptor expression at the cell surface was used as an independent variable to modulate the signal 'strength' for each ITAM variant so that we could directly compare NFAT-mediated GFP expression at equivalent input levels. We plotted the fraction of responding cells as a function of receptor expression at two different rapalog concentrations. For both levels of total input signal controlled by rapalog concentration, it was evident that increasing ITAM multiplicity decreased the number of receptors required to cause an equivalent fraction of activated cells (Fig. 1, H and I). By fitting these datasets, we could quantify this effect on receptor potency directly by calculating the EC_{50}, the cell input required for a half-maximal response (Fig. 1, J and K).

The potency of a signaling response is defined as the combination of the affinity and efficacy of ligand binding to a receptor. Given that all the synthetic receptors bear an identical ligand-binding domain, and so have equivalent affinity, the increased potency with more ITAMs must be the result of increased efficacy. This suggested that the primary effect of the increased number of ITAMs is to improve the likelihood, or efficiency, of productive signal transduction on ligand binding and was not found to substantially amplify the input signal *per se*. It was nonetheless possible for a decreased number of ITAMs to elicit the same response as the complete TCR construct but this required a greater number of receptors to be engaged to drive an equivalent response. This showed that low potency could be overcome by increasing the total ligand input to the cell, at least for the outputs we measured.

Increased receptor ITAM number synchronizes initiation of T-cell signaling

The previous data demonstrated that the number of ITAMs within the receptor affected the efficiency with which the receptor transduced ligand binding to the proximal signaling network. If this were the case, then it should have a significant effect on the rate at which signaling was

initiated at the receptor, with a higher number of ITAMs predicated to drive more efficient, or synchronous signaling. We thought that this effect should be evident in the kinetics of the early events of receptor signaling in the T cells. To test this hypothesis, we used one of the earliest readouts of receptor stimulation in T-cell activation, which is the increased concentration of intracellular Ca^{2+} ions. Importantly, this signaling flux can be measured at single-cell resolution by flow cytometry using the Indo-1 ratiometric Ca^{2+} indicator (*16*).

Jurkat T cells expressing equivalent levels of the synthetic receptors (fig. S4A) were first conjugated with FRB-expressing B cells in the absence of the rapalog drug. These cell conjugates could then be gated on by flow cytometry, a process that was independent of the particular receptor expressed (fig. S4B). The Indo-1 ratio in these conjugates, which reports the intracellular Ca^{2+} concentration, was measured for an initial period to define a baseline ratio before the rapalog drug was added, which synchronously initiated receptor signaling (Fig. 2A). From this data, we quantified the temporal evolution of the activated fraction of cells (Fig. 2, B and C) and the mean Indo-1 ratio of the activated population (Fig. 2, D and E). The clear result was that the number of ITAMs present on the receptor had a potent effect on the rate at which T cells responded to stimulation, at both the 'low' (Fig. 2, B and D) and 'high' (Fig. 2, C and E) rapalog concentrations, with a strong correlation between the increased ITAMs per receptor and the synchrony of the activation response. This can be better illustrated by taking the differential of these plots to derive the rate of activation, showing that increased ITAMs leads to a sharpened or more 'normal' temporal distribution of receptor triggering (Fig. 2, B to E). As for the previous experiments, this effect can be solely ascribed to the number of ITAMs present on the receptor, as both receptor expression and ligand affinity was consistent between all experiments.

We could not collect the Ca^{2+} flux data beyond ~8 min due to technical limitations. This precluded integrating over the time-varying data to extract the overall output response to know whether the

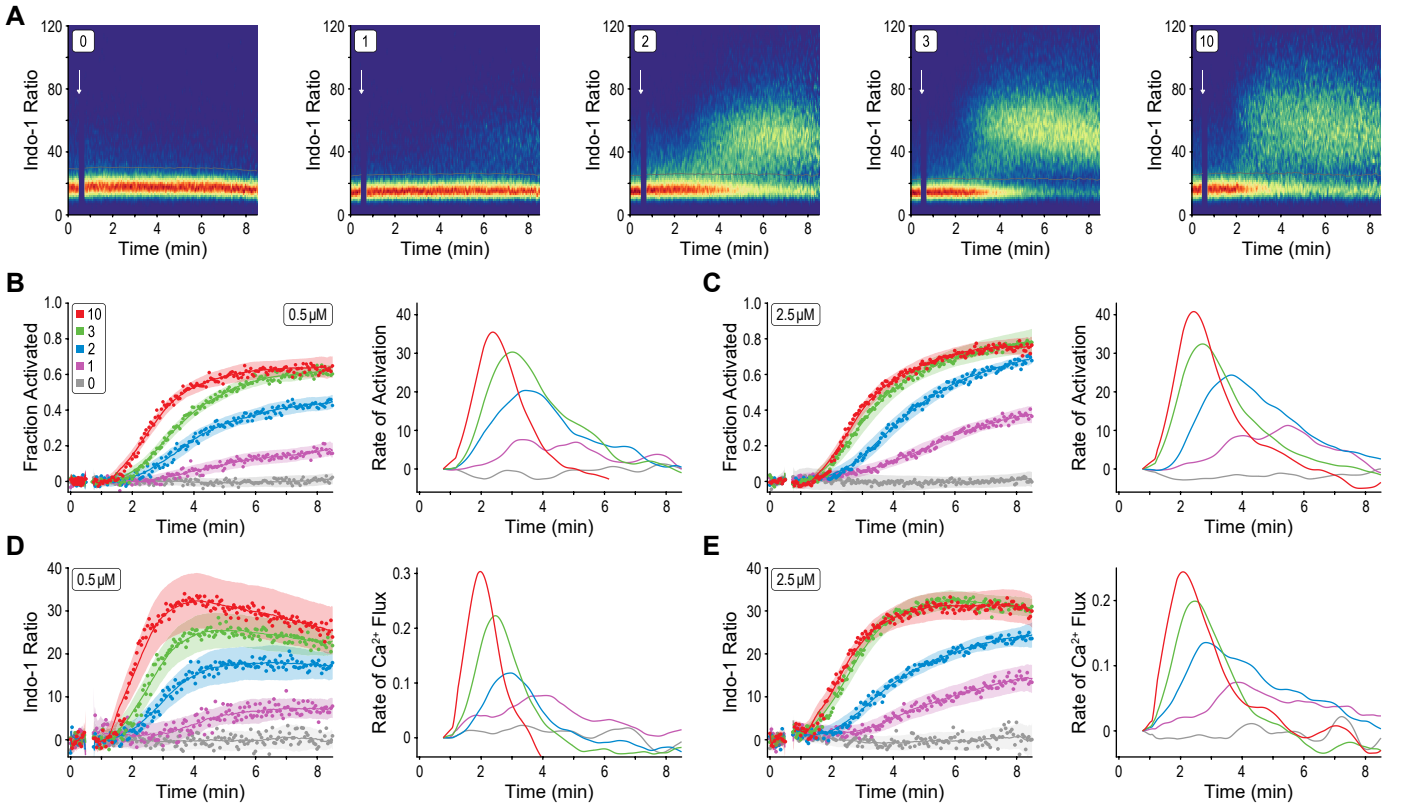

Fig. 2. Increasing ITAM multiplicity drives more synchronous T-cell activation. (**A**) Jurkat T cells expressing the synthetic receptor were loaded with the Ca^{2+} indicator Indo-1 before conjugation with FRB-expressing Raji B cells. T cells were activated by 2.5 μM rapalog addition (white arrow) and the Ca^{2+} flux, presented as Indo-1 fluorescence ratio, was recorded with time by flow cytometry. Plots show the flux profile for the synthetic receptors bearing the designated number of ITAMs (white box). The binned density at each point is denoted by color scale. The solid line marks the boundary between responding and non-responding cells used in the subsequent analyses. (**B** and **C**) The fraction of T cells activated over time was calculated when cells expressing the synthetic receptor with number of ITAMs shown in legend were synchronously initiated at 30 s using 0.5 μM (B) or 2.5 μM (C) rapalog. The mean of three independent experiments is shown for each ITAM variant, along with a bounding area representing SEM. Data points have been decimated and the moving-average fit and bounding area smoothed for visual clarity. The panels on right show the derived rate of activation (after smoothing) for these datasets. (**D** and **E**) Equivalent datasets as in B and C, now showing the mean Indo-1 ratio of the activated fraction of T cells over time when synchronously initiated at 30 s using 0.5 μM (D) or 2.5 μM (E) rapalog. The mean of three independent experiments is shown for each ITAM variant, along with a bounding area representing SEM. Data points have been decimated and the moving-average fit and bounding area smoothed for visual clarity. The panels on right show the derived rate of activation (after smoothing) for these datasets.

increase in the instantaneous Indo-1 ratio with greater ITAM multiplicity (Fig. 2, D and E) was simply the result of the more synchronized response. A model dataset where an invariant individual cellular response is combined with varying temporal distributions for activation could replicate the datasets well (fig. S4C), suggesting that the absolute Ca^{2+} flux of individual cells could be constant despite altered ITAM multiplicity. Nonetheless, we cannot exclude the possibility that for the Ca^{2+} flux during T-cell activation, there is some ITAM-mediated amplification of receptor signaling, perhaps driven by the positive feedback loop of Ca^{2+}-induced Ca^{2+} entry into the cell through CRAC channels.

Effect of ITAM multiplicity on signaling through the MAPK pathway

The previous experiments demonstrated that increased ITAM multiplicity on the synthetic receptors caused an increased fraction of cells to be activated, with signaling initiated in a more synchronous fashion. We next wanted to investigate whether these responses could be observed as receptor activation was propagated through the intracellular signaling networks. To measure this, we used phosphorylation of ERK (a MAP kinase) as an output for intracellular T-cell signaling that is distinct from both the Ca^{2+} flux and NFAT signaling pathways.

We followed a similar strategy as for the Ca^{2+} flux experiments, where synthetic receptor-expressing T cells were conjugated with FRB-presenting B cells in the absence of the rapalog drug. Subsequent addition of the rapalog initiated synchronous activation of receptor signaling that is expected to drive ERK phosphorylation, a functional output that can be measured at the single-cell level using intracellular cytometry staining. We found that after 5 min of signaling, ERK phosphorylation was readily detectable for both rapalog concentrations used previously (Fig. 3, A and B). Through an equivalent analysis as used for the NFAT-mediated signaling output (fig. S1C), we could again show that the effect of higher receptor ITAM multiplicity was to increase the fraction of activated cells (Fig. 3C), with almost no effect on the mean phosphorylation of ERK (Fig. 3D). This result agrees with a previous study that found ERK phosphorylation shows a ‘digital’ response to graded T-cell activation (*17*).

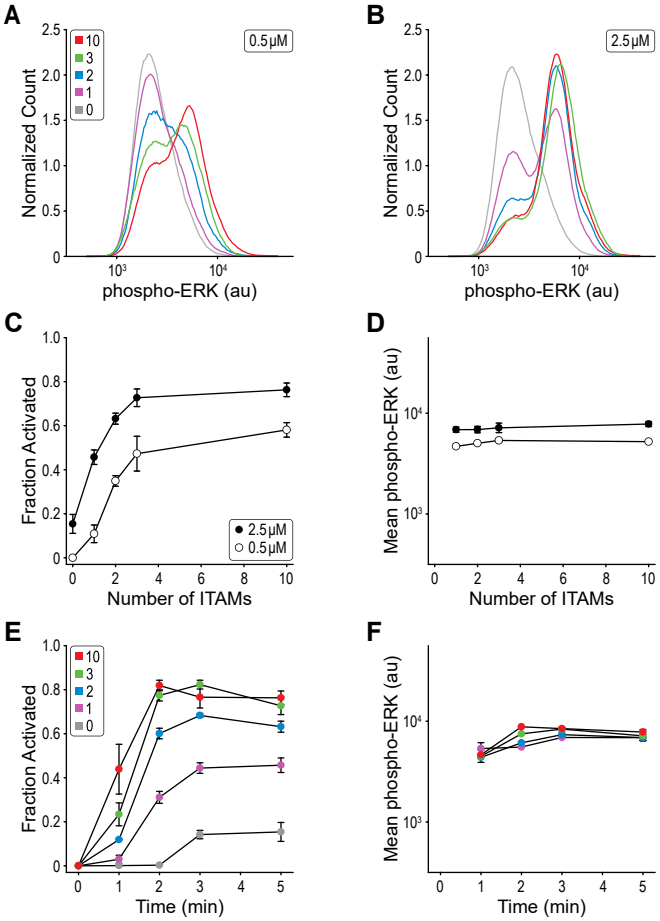

Fig. 3. Effect of increased ITAM multiplicity on ERK phosphorylation kinetics. (**A** and **B**) Jurkat T cells expressing equivalent levels of the synthetic receptor encoding the number of ITAMs shown in legend were conjugated with FRB-expressing Raji B cells. Cell conjugates were then incubated in the presence of 0.5 μM (A) or 2.5 μM (B) rapalog for 5 min before fixation and intracellular staining for phospho-ERK1/2. Representative flow cytometry data from one experiment of T cell activation is shown, where the fluorescence intensity distribution is derived solely from cell conjugates. (**C** and **D**) Data from A and B were used to calculate the fraction of T cells that had been activated (C) and the mean phospho-ERK intensity of this activated fraction (D) at the rapalog concentration shown in the legend. The mean of three independent experiments is shown for each data point, with error bars representing SEM. (**E** and **F**) An equivalent experiment as presented in (B) was performed but now 2.5 μM rapalog was added for times ranging from 0 – 5 min prior to fixation. The fraction of activated T cells at each time-point is shown (E), along with the mean phospho-ERK intensity of this activated fraction (F). The legend indicates the number of ITAMs encoded by the synthetic receptor expressed in the T cells. The mean of three independent experiments is shown for each data point, with error bars representing SEM.

Because of the rapid kinetics of ERK phosphorylation, we wanted to know whether we could also observe the more synchronous signaling observed in the Ca^{2+} flux data when more ITAMs were encoded by the receptor. We therefore measured ERK phosphorylation at earlier time points to follow its kinetics. In agreement with our previous results, we found that greater ITAM multiplicity drove a more rapid response, which was evident especially at 2 min after rapalog addition (Fig. 3E and fig. S5) and the mean ERK phosphorylation became essentially equivalent once the dynamics reached equilibrium after ~3 min (Fig. 3F).

Overall, our data measuring ERK phosphorylation confirmed our previous findings on the effect of ITAM multiplicity on both the increased synchrony of signaling and the fraction of cells that become activated.

ZAP70 kinase activation primarily depends on autophosphorylation

The preceding experiments showed that the number of ITAMs present on the receptor was predominantly affecting the efficiency of transducing the ligand binding event into a downstream signal. What enhancement could high ITAM multiplicity then have on receptor potency, if not through downstream signal amplification? One explanation could be that multiple binding sites within a single antigen receptor are required to bring multiple ZAP70 kinases into close physical proximity. This could be important for ZAP70 because full activation of its kinase activity is known to require phosphorylation of Y493 in its kinase domain activation loop (*18*). For this explanation to be correct, the effect of high ITAM multiplicity is predicated on the requirement for ZAP70 activation to occur through trans-autophosphorylation (Fig. 4A). However, this question remains unresolved, and there is limited experimental evidence for an autophosphorylation mechanism for ZAP70 activation (*19*, *20*). Indeed, a recent study predicted that the ZAP70 activation loop sequence should be a poor substrate for its own kinase domain (*21*) and suggested that ZAP70 is primarily activated by LCK (Fig. 4A).

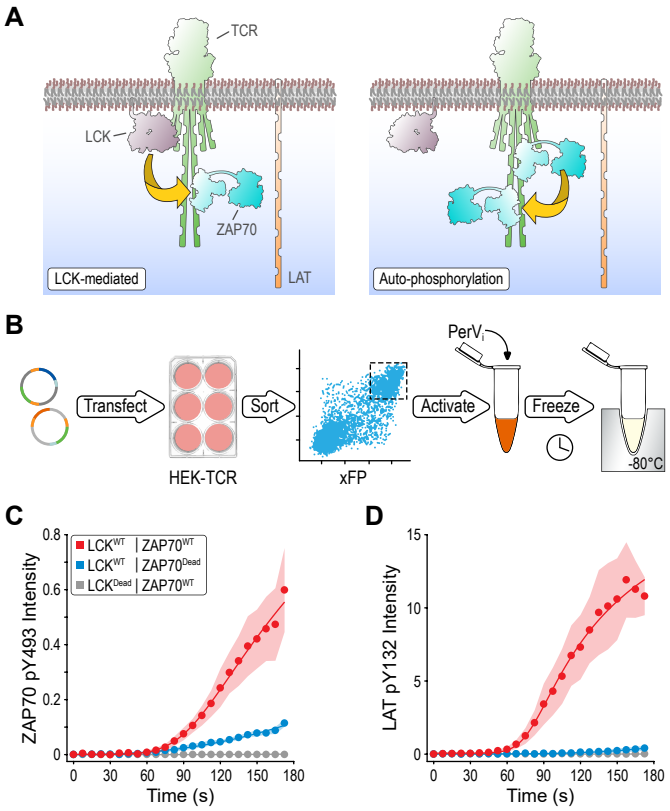

Fig. 4. ZAP70 activation is primarily driven by autophosphorylation. (**A**) Alternative representations for the mechanism of ZAP70 activation through Y493 phosphorylation, which could be driven by LCK-mediated kinase activity (left) or through ZAP70 trans-autophosphorylation (right). (**B**) Schematic of the kinetic experiment. HEK-293T expressing the entire TCR complex were transfected with the minimal components of the TCR triggering apparatus (LCK, ZAP70, LAT, CD45, CSK/CBP), sorted on expressing cells and synchronously activated by inhibiting CD45 phosphatase using pervanadate (PerV$_i$). At defined time-points, aliquots of the activated cells were removed and snap-frozen in tubes pre-frozen in a metal block, before being lysed and analyzed by phospho-western analysis. (**C** and **D**) Plots of the kinetics of ZAP70 phosphorylation at Y493 (C) or LAT phosphorylation at Y132 (D) are presented, when either the wildtype ('WT') or kinase-dead ('Dead') versions of LCK and ZAP70 are expressed in the reconstituted TCR triggering system, as shown in legend. All datasets were collected at 21˚C, and the mean of three independent experiments is shown at each time-point, along with a bounding area representing SEM. Datasets were fit using a logistic function.

We wanted to provide direct evidence as to whether the ZAP70 autophosphorylation was indeed important for its own activation, which would speak to the advantage of high ITAM multiplicity on the TCR. To do this, we used a previously characterized reconstituted cellular system, which relies on expressing the minimal set of proteins (TCR, LCK, ZAP70, CD45, CSK/CBP and LAT) required to recapitulate proximal TCR signaling events in HEK-293T, a non-immune cell-type (*13*). This approach allows us to quantitatively investigate the proximal events of T-cell activation within a cellular system that expresses essentially none of the T-cell proteins that could potentially confound the interpretation of our results (*13*). We therefore measured the kinetics of proximal signaling through the reconstituted protein network, using phosphatase inhibition to synchronously initiate signaling (Fig. 4B and fig. S6A) and quantified the intensity of ZAP70^{Y493} phosphorylation over time by fluorescent phospho-western analysis.

By co-expressing the wildtype forms of both LCK and ZAP70, we could readily observe phosphorylation of ZAP70^{Y493} increasing with time (Fig. 4C). We first confirmed that this measured phosphorylation was solely due to the expressed components, and not any endogenous kinases also present in the reconstituted cells by using a catalytically-inactive mutant of LCK (LCK^{K273R}). This caused ZAP70 phosphorylation to become undetectable (Fig. 4C), confirming the stringent dependence of LCK in the initiation of TCR signaling in the reconstituted system (*13*). However, repeating this assay with a kinase-dead version of ZAP70 (ZAP70^{K369R}) also caused a very substantial reduction in ZAP70^{Y493} phosphorylation (Fig. 4C). We believe this provides direct evidence that ZAP70 activation has a strong dependence on its own kinase activity, with the activation mechanism predominantly relies on ZAP70 trans-autophosphorylation (*22*). This requirement was not absolute though, as there was still some Y493 phosphorylation mediated by LCK when ZAP70 was catalytically inactive (Fig. 4C). This is perhaps an expected requirement to ‘prime’ the bound ZAP70 so that it can initiate the autophosphorylation process. We have

recently demonstrated the requirement for auto-phosphorylation in ZAP70 activation using a complementary assay (*23*).

Both the NFAT-driven reporter (Fig. 1) and Ca^{2+} flux experiments (Fig. 2) depend on the upstream enzymatic activity of the phospholipase PLCγ1 (*24*). This enzyme is recruited to the plasma membrane by binding to LAT^{Y132} when it becomes phosphorylated during proximal TCR signaling (*25*). To confirm that this phosphorylation was dependent on ZAP70 kinase activity, and so would be influenced by ITAM multiplicity, we measured the kinetics of LAT^{Y132} phosphorylation. We found that ZAP70 was indeed the kinase responsible for this modification (Fig. 4D), with LCK showing undetectable phosphorylation of this site over the time period studied (Fig. 4D), as has also been shown recently (*21*).

To see whether the requirement for ZAP70 autophosphorylation could also explain the kinetics of our Ca^{2+} flux (Fig. 2) and phospho-ERK data (Fig. 3), we created network models that invoked the known proximal steps of TCR triggering using BioNetGen (*26*) that could be scaled with receptor ITAM density, and used LAT phosphorylation as a 'readout' of receptor activation (fig. S6, B and C). Using a model that relied on LCK-mediated ZAP70 activation could not readily replicate our experimental data (fig. S6B) but one that relied on ZAP70 autophosphorylation within a single receptor complex could (fig. S6C), which was most evident in the substantial increase in cell output from one to two ITAMs.

Improving CAR activation and discrimination

Chimeric antigen receptors (CARs) are a new class of cancer therapy that use genetically engineered T cells to attack malignant cells. These constructs splice the high affinity binding of antibodies onto the ITAMs of the TCR, including costimulatory motifs to maintain their expression

in the host (fig. S7A). While much work has gone into improving the latter sequences, there has been very limited work on optimizing the signaling potency mediated by the ITAMs (*27*). Current CARs employ the 3 ITAMs from the CD3ζ chain of the TCR, but we hypothesized that the efficiency of CAR activation could be improved by simply increasing the ITAM density of the construct. To do this, we duplicated the CD3ζ sequence to create a 6 ITAM CAR variant (fig. S7A). We also made equivalent versions that had 0-2 ITAMs as well, to quantify the relationship between the number of ITAMs and the CAR-mediated response.

As a proof-of-principle, we used a CAR that is reactive to CD19, a B-cell specific surface protein that has been previously used to target CAR-expressing T cells against lymphoblastic leukemias (*28*, *29*). We transduced human primary $CD4^+$ T cells (fig. S7B) to express α-CD19 CAR variants with 0-6 ITAMs. As surrogate target cells, we used K562 myeloma cells that were transduced to express different levels of the CD19 antigen, spanning over the normal range of CD19 expression (fig. S7C). CAR-T cells were conjugated with target cells for 24 hours to drive CD19-induced T-cell activation that was quantified by increased expression of CD137 (fig. S7D), a robust marker of activation that correlates well with cell proliferation (*30*).

As expected, the 'standard' CAR construct harboring 3 ITAMs caused activation of transduced T cells when mixed with target cells presenting all three antigen densities (Fig. 5A). However, increasing the number of ITAMs from 3 to 6 increased the efficiency of T-cell activation by ~15% for all target cells (Fig. 5, A and D). By using the same analysis as the for the synthetic receptors, we again found that the effect of increased ITAM number primarily caused an increase in the fraction of activated cells (Fig. 5B) and not the absolute level of the cell output (Fig. 5C). This effect held true for all three levels of CD19 expression on the target cells (Fig. 5, B and C), although activation was clearly enhanced with higher target density suggesting CAR-mediated signaling was not saturated. Similar results were found using CD69 as the readout for T-cell activation,

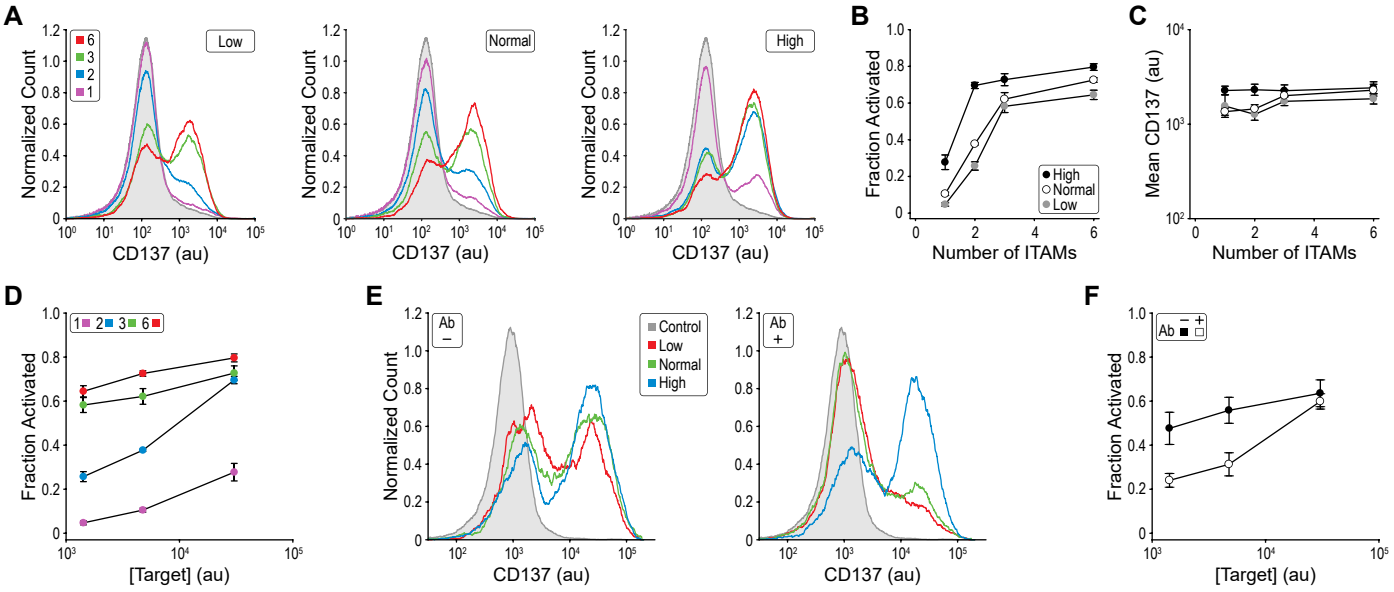

Fig. 5. Chimeric antigen receptor potency can be modulated by ITAM multiplicity. (**A**) Human CD4⁺ T cells expressing a CD19-reactive CAR with the number of ITAMs shown in legend were mixed with K562 target cells expressing the designated level of CD19. The expression of CD137 (4-1BB) activation marker was determined 24 hours later by flow cytometry, shown as representative histograms from one experiment. CAR expression in T cells was equivalent between all ITAM variants. (**B** and **C**) Data from A were used to calculate the fraction of T cells that had been activated (B) and the mean CD137 intensity of this activated fraction (C) when T cells were stimulated with target cells expressing the level of CD19 shown in the legend. The mean of three independent experiments is shown for each data point, with error bars representing SEM. (**D**) The data in B is replotted to show the effect of target density on the fraction of activated cells, for each CAR expressing the number of ITAMs shown in legend. (**E**) T cells expressing the wild-type CAR (3 ITAMs) were activated with target cells, either in the absence or presence of a blocking antibody against CD19. Legend shows the target cells that were used for each dataset. Representative flow cytometry plots of CD137 expression are presented from one experiment. (**F**) Data from E were used to calculate the fraction of CAR-expressing T cells that had been activated by target cells expressing different CD19 levels, performed either in the absence or presence of a blocking α-CD19 antibody, as shown in legend. The mean of three independent experiments is shown for each data point, with error bars representing SEM.

although it appeared the activation period allowed for subsequent down-regulation of CD69, clearly evident in the 'high' target-cell data, which slightly confounded the analysis (fig. S7E-G).

An unanticipated result from this dataset was that by decreasing the number of ITAMs in the receptor construct from 3 to 2 ITAMs, the CAR-T cells were now substantially more selective for target cells over-expressing the CD19 target antigen (Fig. 5D), something that CARs are not currently optimized for. This agreed with the synthetic receptors experiments described above, which showed that equivalent T-cell activation with fewer ITAMs can only be achieved with more engaged receptors, which would be the case for the target cells over-expressing CD19. To expand on this finding, we reasoned that manipulating the available target density on the CD19-expressing target cells could be an alternative means to make the CAR-T cells respond more selectively to K562 over-expressing the target protein, so sparing target cells expressing more-physiological CD19 levels. To achieve this, we repeated the experiment using the original CAR with 3 ITAMs but now included the full-length antibody that the α-CD19 CAR is constructed from during T-cell activation, to sterically 'block' most of the available target sites. We hypothesized that this would artificially shift the effective target densities to a regime where the CAR could be more selective towards target cells over-expressing CD19. This was indeed what we found (Fig. 5E); antibody addition 'protected' the target cells expressing physiological levels of CD19 while allowing the over-expressing cells to still be targeted (Fig. 5F).

Discussion

We have developed a synthetic receptor system to quantitatively investigate how the number of ITAMs encoded by a cell surface receptor modulates its ability to drive intracellular signaling in T cells. We found that greater receptor ITAM multiplicity enhanced the potency of the receptor, by increasing the efficacy, or transduction efficiency of ligand binding being converted into an intracellular signal. This effect manifested as an increase in the fraction of T cells that became activated with a greater number of ITAMs with a more synchronous initiation of downstream signaling, and was consistent over five distinct downstream signaling outputs, providing strong support for our conclusions. Through reconstitution experiments, we showed that there is a substantial requirement for autophosphorylation to drive ZAP70 kinase activity, which could provide a mechanistic explanation for the increased efficacy observed with high ITAM multiplicity. Unfortunately, it was not technically possible to investigate ZAP70 activation at the single-cell level to directly confirm this hypothesis.

We then tested the idea that the number of ITAMs increased receptor potency by demonstrating that we could improve the therapeutic potential of CARs. We found that increased ITAM count on an α-CD19 CAR led to improved activation of primary human T cells, a result that should be applicable to all current CARs being trialed and the effect is likely to be significantly higher when the target antigen is expressed at low levels. Conversely, decreasing the number of ITAMs, or using different ITAM sequences with weaker binding affinities (*31*) could be an interesting new avenue to provide some selectivity to target expression levels.

These findings contrast with the prevailing view that ITAM multiplicity is principally for intracellular signal amplification, which should lead to greater absolute levels of signaling output. We believe our experiments at single-cell resolution demonstrate that this is not the primary effect of high number of ITAMs. Instead, we find that greater ITAM multiplicity leads to a decrease in

the number of triggered receptors required to cause a half-maximal output response. Equivalent levels of signaling were possible with fewer ITAMs but this required more receptors to be engaged. By only measuring the mean response of a population of T cells, as essentially all other experiments on ITAM number have been done, it would not be possible to separate these two explanations. Our results suggest that ITAM multiplicity of the receptor influences the conversion of ligand binding into an intracellular signal. Although it could be argued that simply having more bound ZAP70 is amplification *per se*, we believe this is not an appropriate use of the term because of the change in input modality, with amplification normally only defined as an increase in a signal amplitude.

A key advantage of our experiments using the synthetic receptor is that a gain-of-function approach to investigate ITAM multiplicity obviates the need to directly disrupt the underlying signaling network, which can often lead to unintended consequences such as systemic adaptation. There are of course caveats to our approach too. By expressing the synthetic receptors in an endogenous T-cell line we are inherently increasing the total density of ITAMs at the cell surface, which could alter basal signaling. We were therefore careful not to over-express the receptor, which increased the total ITAM density by no more than ~10% at the highest receptor expression used. The synthetic receptor also relied on the FKBP/FRB interaction that has a higher affinity than the normal TCR/pMHC equivalent, although the kinetics of the FKBP unbinding under tension have never been measured and so may not be so different to that for pMHC dissociation. The presence of the endogenous TCR in our synthetic receptor-expressing T cells could potentially lead to signal augmentation by co-opting these receptors. However, we saw no evidence for wildtype TCR downregulation in our assays even with potent stimulation, suggesting that only the engaged receptors were providing signal input to the cells.

While the synthetic receptors used in this study may not replicate all the features of the endogenous TCR, we believe the work presented here can explain the requirement for 10 ITAMs being present within the TCR complex. Why does the TCR have this requirement? The unique aspect of TCR-mediated signaling is that it must function at very high sensitivity, with potentially only a few ligands being sufficient to drive cell activation (*32*, *33*). To achieve this, the TCR must be able to convert cognate pMHC binding events as effectively as possible into a triggered receptor; this efficacy in signal transmission across the plasma membrane is then derived from the high ITAM multiplicity, something not required for most other immune receptors. Furthermore, having the ITAMs distributed over multiple chains, rather than encoded by a single large sequence might increase the efficiency of receptor triggering by increasing the effective local concentration of ZAP70 binding sites. It is also possible ligand-induced receptor clustering (*34*) or pre-formed TCR 'nanoclusters' in the plasma membrane (*35*) could further enhance the efficacy of receptor triggering to low levels of pMHC ligands by increasing the effective number of ITAMs that could drive autophosphorylation and hence proximal signaling.

Materials and Methods

Construct design and cell transduction

All DNA vector constructs, cell culture, and transient and lentiviral transduction procedures are detailed in the Supplementary Methods.

Chemically-inducible synthetic receptor system

Construction of the vectors for the FKBP-CD86-CD3ζ receptor (previously described as $FKBP^{Ex}\zeta^{Int}$), its ligand, FRB^{Ex}, and the Raji B-cell line expressing this ligand have been previously described (*13*), although the synthetic receptor now included an HA-epitope at the mature N-terminus for quantification of expression. The first Tyr in each ITAM was mutated to Phe to sequentially decrease the number of ITAMs. To engineer a receptor complex with 10 ITAMs, we fused FKBP to the mature N-terminus of the TCRα sequence from Jurkat T cells (along with an HA-epitope), which was incorporated into the endogenous Jurkat TCR complex through competition with the wildtype equivalent TCRα chain. A clonal Jurkat derivative (J.NFAT) was created that expressed GFP on TCR stimulation using NFAT-response elements, as well as constitutively expressing the fluorophore iRFP713 for identification. The synthetic receptors were transduced in J.NFAT cells and expression was measured using the HA-epitope, which could be quantified using fluorescent calibration beads as described in the Supplementary Methods.

Calcium flux and phospho-ERK analysis

Synthetic receptor-expressing T cells were loaded with Indo-1, a fluorescent Ca^{2+} indicator prior to conjugation with Raji B cells expressing the cognate binding domain (FRB^{Ex}). Cell conjugates were gated on by flow cytometry and the Ca^{2+} flux of these cell conjugates was measured, after baseline acquisition, after the rapalog drug was added. We used a similar approach for measuring phospho-ERK levels, where cell conjugates were first formed in the absence of the rapalog drug. The conjugates were then incubated with the rapalog for a defined period at 37°C before fixing using 4% formaldehyde. Fixed cells were then methanol-extracted and subsequently stained with

a directly-conjugated fluorescent antibody to phospho-Erk1/2 (T202/Y204). Further details, including data analysis are detailed in the Supplementary Methods.

Downstream cellular activation

J.NFAT cells expressing the appropriate synthetic receptor were conjugated to Raji-FRB^{Ex} cells for 30 min as described for the Ca^{2+} flux assay, except that the cells were conjugated in medium that included the rapalog drug at the prescribed concentration. Conjugates were then cultured for 16 hours to allow activation-induced expression of GFP from the NFAT-responsive promoter. The supernatant of the activated cells was also collected as this point to assay for IL-2 cytokine secretion. Cells were stained with a fluorescently-conjugated antibody against the HA-epitope prior to running the sample on a flow cytometer to measure both receptor and GFP expression. Further details, including data analysis are given in the Supplementary Methods.

Cellular reconstitution of TCR phosphorylation kinetics

HEK-293T cells were transduced to express all the proteins required to reconstitute the proximal events of TCR triggering, as described previously (*13*). HEK-TCR cells, which stably expressed the entire TCR complex (1G4 clone), were transiently transfected and sorted by flow cytometry to purify a homogeneous population of cells expressing all components (LCK, ZAP70, LAT, CD45 and CSK/CBP), which were fluorophore tagged for detection. These sorted cells were then activated at 21°C using pervanadate. Aliquots of the cells were taken at defined time-points and rapidly quenched by snap-freezing. Frozen samples were lysed on ice, pelleted to remove perinuclear material and heated at 70°C in reduced LDS sample buffer. Samples were subjected to gel electrophoresis, before blotting onto nitrocellulose and probing for the required (phospho-) protein by Western analysis in conjunction with fluorescent secondary antibodies. Blots were imaged using an Odyssey Imaging system. Further details, including band quantification and data analysis are detailed in the Supplementary Methods.

Modeling effect of ITAM number on receptor triggering

BioNetGen (*26*) was used to model TCR triggering. The two Tyr residues of an ITAM were modeled as a single phosphorylation event to minimise complexity. Up to 6 ZAP70-binding sites could be computed (over ~20 hours) but more than this became unfeasible. The code used to model the network, along with further details are detailed in the Supplementary Methods.

Chimeric antigen receptor activation

The anti-CD19 chimeric antigen receptor (CAR), including mutations of the ITAMs of the CD3ζ sequence as described for the synthetic receptor above, was lentivirally transduced into human primary $CD4^+$ T cells and left to proliferate over ~10 days until there was a clear decrease in cell volume, judged by scatter on a flow cytometer. To construct a CAR variant with 6 ITAMs, the CD3ζ intracellular sequence was duplicated, and all synonymous mutations in one half were made. This sequence was synthesized and inserted into the CAR vector. K562 target cells were transduced to express the CD19 protein using different promoters to drive differential surface densities. Cell sorting was used to select three different target cell lines. T cells were conjugated with these target cells over 24 hours and stained with fluorescently-labeled antibodies against CD137 and CD3 and were then measured by flow cytometry. When required, the target cells were pre-incubated with an anti-CD19 antibody to block the CAR epitope, and the antibody was present throughout the subsequent incubations. Further details, including data analysis are detailed in the Supplementary Methods.

Supplementary Materials

fig. S1. Supplementary data for downstream output using synthetic receptors

fig. S2. Effect of ITAM multiplicity on IL-2 cytokine secretion

fig. S3. Representative cytometry data for downstream output using synthetic receptors

fig. S4. Supplementary data for Ca^{2+} flux data using synthetic receptor

References

1. P. A. Merwe, O. Dushek, P. A. van der Merwe, Mechanisms for T cell receptor triggering. *Nat. Rev. Immunol.* **11**, 47–55 (2011).
2. P. E. Love, S. M. Hayes, ITAM-mediated signaling by the T-cell antigen receptor. *Cold Spring Harb. Perspect. Biol.* **2**, a002485 (2010).
3. J. Holst *et al.*, Scalable signaling mediated by T cell antigen receptor-CD3 ITAMs ensures effective negative selection and prevents autoimmunity. *Nat. Immunol.* **9**, 658–666 (2008).
4. C. S. Guy *et al.*, Distinct TCR signaling pathways drive proliferation and cytokine production in T cells. *Nat. Immunol.* **14**, 262–270 (2013).
5. Z. Grossman, W. E. Paul, Dynamic Tuning of Lymphocytes: Physiological Basis, Mechanisms, and Function. *Annu. Rev. Immunol.* **33**, 677–713 (2015).
6. L. Ardouin *et al.*, Crippling of CD3-ζ ITAMs does not impair T cell receptor signaling. *Immunity*. **10**, 409–420 (1999).
7. S. Hwang *et al.*, TCR ITAM multiplicity is required for the generation of follicular helper T-cells. *Nat. Commun.* **6**, 6982 (2015).
8. H. Mukhopadhyay *et al.*, Multisite Phosphorylation Modulates the T Cell Receptor ζ -Chain Potency but not the Switchlike Response. *Biophys. J.* **110**, 1896–1906 (2016).
9. J. R. James, M. I. Oliveira, A. M. Carmo, A. Iaboni, S. J. Davis, A rigorous experimental framework for detecting protein oligomerization using bioluminescence resonance energy transfer. *Nat. Methods*. **3**, 1001–6 (2006).
10. J. Chen, X. F. Zheng, E. J. Brown, S. L. Schreiber, Identification of an 11-kDa FKBP12-rapamycin-binding domain within the 289-kDa FKBP12-rapamycin-associated protein and characterization of a critical serine residue. *Proc. Natl. Acad. Sci. U. S. A.* **92**, 4947–51 (1995).
11. J. Choi, J. Chen, S. L. Schreiber, J. Clardy, Structure of the FKBP12-rapamycin complex interacting with the binding domain of human FRAP. *Science*. **273**, 239–42 (1996).
12. S. Faivre, G. Kroemer, E. Raymond, Current development of mTOR inhibitors as anticancer agents. *Nat. Rev. Drug Discov.* **5**, 671–688 (2006).
13. J. R. James, R. D. Vale, Biophysical mechanism of T-cell receptor triggering in a reconstituted system. *Nature*. **487**, 64–9 (2012).
14. M. C. Castellanos *et al.*, Expression of the leukocyte early activation antigen CD69 is regulated by the transcription factor AP-1. *J Immunol*. **159**, 5463–5473 (1997).
15. K. A. Allison *et al.*, Affinity and dose of TCR engagement yield proportional enhancer and gene activity in CD4+ T cells. *Elife*. **5**, 1–28 (2016).
16. G. Grynkiewicz, M. Poenie, R. Y. Tsien, A new generation of Ca2+ indicators with greatly improved

fluorescence properties. *J. Biol. Chem.* **260** (1985), pp. 3440–3450.

17. G. Altan-Bonnet, R. N. Germain, Modeling T cell antigen discrimination based on feedback control of digital ERK responses. *PLoS Biol.* **3**, e356 (2005).
18. B. B. Au-Yeung *et al.*, The structure, regulation, and function of ZAP-70. *Immunol. Rev.* **228**, 41–57 (2009).
19. M. Mallaun, G. Zenke, E. Palmer, A discrete affinity-driven elevation of ZAP-70 kinase activity initiates negative selection. *J. Recept. Signal Transduct. Res.* **30**, 430–43 (2010).
20. H. Wang *et al.*, ZAP-70: an essential kinase in T-cell signaling. *Cold Spring Harb. Perspect. Biol.* **2**, a002279 (2010).
21. N. H. Shah *et al.*, An electrostatic selection mechanism controls sequential kinase signaling downstream of the T cell receptor. *Elife*. **5** (2016), doi:10.7554/eLife.20105.
22. T. Brdicka, T. A. Kadlecek, J. P. Roose, A. W. Pastuszak, A. Weiss, Intramolecular Regulatory Switch in ZAP-70: Analogy with Receptor Tyrosine Kinases. *Mol. Cell. Biol.* **25**, 4924–4933 (2005).
23. A. Liaunardy-Jopeace, B. L. Murton, M. Mahesh, J. W. Chin, J. R. James, *Nat. Struct. Mol. Biol.*, in press, doi:10.1038/nsmb.3492.
24. G. Fu *et al.*, Phospholipase Cγ1 is essential for T cell development, activation, and tolerance. *J. Exp. Med.* **207**, 309–18 (2010).
25. L. Balagopalan, N. P. Coussens, E. Sherman, L. E. Samelson, C. L. Sommers, The LAT story: a tale of cooperativity, coordination, and choreography. *Cold Spring Harb. Perspect. Biol.* **2**, 1–23 (2010).
26. J. R. Faeder, M. L. Blinov, W. S. Hlavacek, Rule-based modeling of biochemical systems with BioNetGen. *Methods Mol. Biol.* **500**, 113–67 (2009).
27. J. S. Bridgeman *et al.*, CD3ζ-based chimeric antigen receptors mediate T cell activation via cis- and trans-signalling mechanisms: implications for optimization of receptor structure for adoptive cell therapy. *Clin. Exp. Immunol.* **175**, 258–67 (2014).
28. D. L. Porter, B. L. Levine, M. Kalos, A. Bagg, C. H. June, Chimeric antigen receptor-modified T cells in chronic lymphoid leukemia. *N. Engl. J. Med.* **365**, 725–33 (2011).
29. C. Imai *et al.*, Chimeric receptors with 4-1BB signaling capacity provoke potent cytotoxicity against acute lymphoblastic leukemia. *Leukemia*. **18**, 676–84 (2004).
30. M. Wolfl *et al.*, Activation-induced expression of CD137 permits detection, isolation, and expansion of the full repertoire of CD8+ T cells responding to antigen without requiring knowledge of epitope specificities. *Blood*. **110**, 201–210 (2007).
31. H. Mukhopadhyay, S.-P. Cordoba, P. K. Maini, P. A. van der Merwe, O. Dushek, Systems model of T cell receptor proximal signaling reveals emergent ultrasensitivity. *PLoS Comput. Biol.* **9**, e1003004 (2013).

32. Q.-J. Li *et al.*, CD4 enhances T cell sensitivity to antigen by coordinating Lck accumulation at the immunological synapse. *Nat. Immunol.* **5**, 791–799 (2004).
33. D. J. Irvine, M. A. Purbhoo, M. Krogsgaard, M. M. Davis, Direct observation of ligand recognition by T cells. *Nature*. **419**, 845–9 (2002).
34. M. J. Taylor, K. Husain, Z. J. Gartner, S. Mayor, R. D. Vale, A DNA-Based T Cell Receptor Reveals a Role for Receptor Clustering in Ligand Discrimination. *Cell*. **169**, 108–119.e20 (2017).
35. S. V Pageon *et al.*, Functional role of T-cell receptor nanoclusters in signal initiation and antigen discrimination. *Proc. Natl. Acad. Sci. U. S. A.* **113**, E5454-63 (2016).

Acknowledgments

This work was supported by a Sir Henry Dale Fellowship (JRJ) jointly funded by the Wellcome Trust and the Royal Society (Grant Number: 099966/Z/12/Z).

Figure Legends

Fig. 1. T-cell signaling potency is enhanced by greater ITAM multiplicity

(**A**) Schematic of the synthetic receptors. For receptors encoding 0-3 ITAMs, the FKBP domain was expressed at the extracellular terminus of CD86 and fused to the intracellular sequence of CD3ζ, with point mutations used to disable the ITAMs when required. For the receptor with 10 ITAMs, the FKBP domain was expressed at the extracellular terminus of the TCRα chain, which was then incorporated into the complete endogenous TCR complex.

(**B**) Schematic of synthetic receptor triggering, with proteins approximately to scale. The receptor is expressed in T cells in the presence of endogenous TCR. Conjugation with cells presenting FRB, the cognate FKBP ligand, drives receptor engagement but only in the presence of the rapalog drug (AP21967). This leads to receptor triggering through LCK-mediated phosphorylation of the receptor and the subsequent recruitment of the cytoplasmic kinase ZAP70 and its activation, shown as an 'opening' of the structure, which causes phosphorylation of proteins such as LAT that initiate downstream signaling.

(**C** and **D**) Jurkat T cells expressing the synthetic receptor encoding the number of ITAMs shown in legend were activated with FRB-expressing Raji B cells in the presence of 0.5μM (C) or 2.5 μM (D) rapalog. Representative flow cytometry data from one experiment of T-cell activation is shown, measured by NFAT-mediated GFP expression, with cells gated for equivalent receptor surface expression.

(**E** and **F**) Data from C and D were used to calculate the fraction of T cells that had been activated (E) and the mean GFP intensity of this activated fraction (F) at the rapalog concentration shown in the legend. The mean of three independent experiments is shown for each data point, with error bars representing SEM.

(**G**) Density plots of activation-induced GFP expression against synthetic receptor expression with differing ITAM multiplicity (white box). Vertical lines denote the range of receptor expression analyzed and the horizontal dashed line shows the threshold for designating a cell as activated.

(**H** and **I**) The fraction of activated Jurkat T cells plotted against receptor expression is shown for all variants of the synthetic receptor in the presence of 0.5μM (H) or 2.5 μM (I) rapalog. Beads with known amounts of fluorophores were used to convert relative fluorescence data from the flow cytometer to absolute surface density. The mean of three independent experiments is shown at each binned expression level, along with a bounding area representing SEM. Datasets are fit using a logistic function.

(**J** and **K**) The receptor density required to cause half-maximal cell activation (EC_{50}) was calculated from datasets (H and I) and is shown as a function of the number of ITAMs encoded by the receptor in the presence of 0.5 μM (J) or 2.5 μM (K) rapalog. A 95% confidence interval is shown as a bounding area.

Fig. 2. Increasing ITAM multiplicity drives more synchronous T-cell activation

(**A**) Jurkat T cells expressing the synthetic receptor were loaded with the Ca^{2+} indicator Indo-1 before conjugation with FRB-expressing Raji B cells. T cells were activated by 2.5 μM rapalog addition (white arrow) and the Ca^{2+} flux, presented as Indo-1 fluorescence ratio, was recorded with time by flow cytometry. Plots show the flux profile for the synthetic receptors bearing the designated number of ITAMs (white box). The binned density at each point is denoted by color scale. The solid line marks the boundary between responding and non-responding cells used in the subsequent analyses.

(**B** and **C**) The fraction of T cells activated over time was calculated when cells expressing the synthetic receptor with number of ITAMs shown in legend were synchronously initiated at 30 s

using 0.5 μM (B) or 2.5 μM (C) rapalog. The mean of three independent experiments is shown for each ITAM variant, along with a bounding area representing SEM. Data points have been decimated and the moving-average fit and bounding area smoothed for visual clarity. The panels on right show the derived rate of activation (after smoothing) for these datasets.

(**D** and **E**) Equivalent datasets as in B and C, now showing the mean Indo-1 ratio of the activated fraction of T cells over time when synchronously initiated at 30 s using 0.5 μM (D) or 2.5 μM (E) rapalog. The mean of three independent experiments is shown for each ITAM variant, along with a bounding area representing SEM. Data points have been decimated and the moving-average fit and bounding area smoothed for visual clarity. The panels on right show the derived rate of activation (after smoothing) for these datasets.

Fig. 3. Effect of increased ITAM multiplicity on ERK phosphorylation kinetics

(**A** and **B**) Jurkat T cells expressing equivalent levels of the synthetic receptor encoding the number of ITAMs shown in legend were conjugated with FRB-expressing Raji B cells. Cell conjugates were then incubated in the presence of 0.5 μM (A) or 2.5 μM (B) rapalog for 5 min before fixation and intracellular staining for phospho-ERK1/2. Representative flow cytometry data from one experiment of T-cell activation is shown, where the fluorescence intensity distribution is derived solely from cell conjugates.

(**C** and **D**) Data from A and B were used to calculate the fraction of T cells that had been activated (C) and the mean phospho-ERK intensity of this activated fraction (D) at the rapalog concentration shown in the legend. The mean of three independent experiments is shown for each data point, with error bars representing SEM.

(**E** and **F**) An equivalent experiment as presented in (B) was performed but now 2.5 μM rapalog was added for times ranging from 0 – 5 min prior to fixation. The fraction of activated T cells at

each time-point is shown (E), along with the mean phospho-ERK intensity of this activated fraction (F). The legend indicates the number of ITAMs encoded by the synthetic receptor expressed in the T cells. The mean of three independent experiments is shown for each data point, with error bars representing SEM.

Fig. 4. ZAP70 activation is primarily driven by autophosphorylation

(**A**) Alternative representations for the mechanism of ZAP70 activation through Y493 phosphorylation, which could be driven by LCK-mediated kinase activity (left) or through ZAP70 *trans*-autophosphorylation (right).

(**B**) Schematic of the kinetic experiment. HEK-293T expressing the entire TCR complex were transfected with the minimal components of the TCR triggering apparatus (LCK, ZAP70, LAT, CD45, CSK/CBP), sorted on expressing cells and synchronously activated by inhibiting CD45 phosphatase using pervanadate ($PerV_i$). At defined time-points, aliquots of the activated cells were removed and snap-frozen in tubes pre-frozen in a metal block, before being lysed and analyzed by phospho-western analysis.

(**C** and **D**) Plots of the kinetics of ZAP70 phosphorylation at Y493 (C) or LAT phosphorylation at Y132 (D) are presented, when either the wildtype ('WT') or kinase-dead ('Dead') versions of LCK and ZAP70 are expressed in the reconstituted TCR triggering system, as shown in legend. All datasets were collected at 21°C, and the mean of three independent experiments is shown at each time-point, along with a bounding area representing SEM. Datasets were fit using a logistic function.

Fig. 5. Chimeric antigen receptor potency can be modulated by ITAM multiplicity

(**A**) Human $CD4^+$ T cells expressing a CD19-reactive CAR with the number of ITAMs shown in legend were mixed with K562 target cells expressing the designated level of CD19. The expression

of CD137 (4-1BB) activation marker was determined 24 hours later by flow cytometry, shown as representative histograms from one experiment. CAR expression in T cells was equivalent between all ITAM variants.

(**B** and **C**) Data from A were used to calculate the fraction of T cells that had been activated (B) and the mean CD137 intensity of this activated fraction (C) when T cells were stimulated with target cells expressing the level of CD19 shown in the legend. The mean of three independent experiments is shown for each data point, with error bars representing SEM.

(**D**) The data in B is replotted to show the effect of target density on the fraction of activated cells, for each CAR expressing the number of ITAMs shown in legend.

(**E**) T cells expressing the wild-type CAR (3 ITAMs) were activated with target cells, either in the absence or presence of a blocking antibody against CD19. Legend shows the target cells that were used for each dataset. Representative flow cytometry plots of CD137 expression are presented from one experiment.

(**F**) Data from E were used to calculate the fraction of CAR-expressing T cells that had been activated by target cells expressing different CD19 levels, performed either in the absence or presence of a blocking α-CD19 antibody, as shown in legend. The mean of three independent experiments is shown for each data point, with error bars representing SEM.

fig. S1. Supplementary data for downstream T-cell activation using synthetic receptors

(**A**) Model data for how signal amplification mediated by ITAM multiplicity might be realized. The first panel shows mock data where successive ITAMs from 1 to 10 (see color legend) increase the signaling output by 12%. This presents as a continuous increase in the signal/noise ratio

between the positive and background peaks but not the fraction of activated cells (second panel). The increase in absolute mean output of the activated fraction and the total population is shown in the third and last panels, respectively.

(**B**) Model data for how increased receptor potency mediated by ITAM multiplicity might be realized. The first panel shows mock data where successive ITAMs from 1 to 10 (see color legend) increase the fraction of cell that are activated, assumed to be a monotonic function (second panel). This presents as a continuous increase in the ratio between the positive and negative peaks but not the signal/noise. The absolute mean output of the activated fraction and the total population is shown in the third and last panels, respectively.

(**C**) Representative examples of how the distribution of activated cells was extracted from the histogram of GFP expression. Data is from the experiment activated using 2.5 μM rapalog with ITAM multiplicity shown in white boxes. The background distribution from Jurkat T cells that had been activated with vehicle control (red area) was used to 'unmix' the histogram, by fitting it under the line through least-squares optimization. This was then subtracted from the total histogram to define the activated or 'positive' distribution (green area). The open circles denote the mean of the total histogram whereas the filled circles show the equivalent mean for the activated distribution.

(**D** and **E**) Jurkat T cells expressing the synthetic receptor with number of ITAMs shown in legend were activated with FRB-expressing Raji B cells in the presence of 0.5μM (D) or 2.5μM (E) rapalog. Representative flow cytometry data for T-cell activation is shown, measured by CD69 expression, with cells gated for equivalent receptor surface expression.

(**F** and **G**) Data from D and E were used to calculate the fraction of T cells that had been activated (F) and the mean CD69 intensity of this activated fraction (G) at the rapalog concentration shown in the legend.

fig. S2. Effect of ITAM multiplicity on IL-2 cytokine secretion

(**A**) Surface expression of the synthetic receptors on T cells used in the IL-2 secretion and phospho-ERK experiments described in the main text, showing that they are essentially equivalent. The number of ITAMs present in each receptor is denoted in the legend.

(**B**) Synthetic receptor-expressing T cells were conjugated with ligand-presenting Raji B cells in the presence of the rapalog drug (concentration shown in legend) and left to activate for 16 hours. The cells were then centrifuged and the supernatant removed for analysis of IL-2 secretion. An ELISA was performed to measure the IL-2 concentration from all samples in technical triplicates, with a known standard used to calibrate absorbance readings to absolute levels of IL-2. The mean of three independent experiments is shown for each data point, with error bars representing SEM.

(**C**) The resuspended cell pellet from the same assay was also subjected to flow cytometry analysis to determine the fraction of GFP-positive T cells at the single-cell level. This was then plotted against the measured IL-2 concentration, which demonstrated a strong correlation between the two downstream signaling outputs.

fig. S3. Representative cytometry data for downstream T-cell activation using synthetic receptors

(**A** and **B**) Representative flow cytometry plots of NFAT-mediated GFP expression (A) or CD69 expression (B) as a function of synthetic receptor expression. Jurkat T cells expressing the receptors were conjugated with FRB-expressing Raji B cells for 16 hours, as described in the main text. The plots show the data from one representative experiment. The columns represent the number of ITAMs present on the synthetic receptor and the rows define the rapalog concentration used to drive receptor-induced activation.

fig. S4. Supplementary data for Ca^{2+} flux data using synthetic receptor

(**A**) Surface expression of the synthetic receptors used in the Ca^{2+} flux experiments described in the main text, showing that they are essentially equivalent. The number of ITAMs present in each receptor is shown in the legend, with the gray histogram showing control staining of untransduced Jurkat T cells.

(**B**) Representative plot of flow cytometry data showing the gating for conjugates formed between iRFP713^{+} Jurkat T cells and mTagBFP^{+} Raji B cells. The boxed area shows the region used to isolate conjugates for the subsequent kinetic analyses.

(**C**) Model data to show that the Ca^{2+} flux data presented in the main text can be explained as the convolution of a uniform individual cellular response and a temporal distribution dictated by receptor ITAM multiplicity. The left panel shows an idealized Ca^{2+} flux profile for a single cell (the impulse response), which was constructed from simple piecewise functions. The middle panel shows different temporal distributions of activation to represent different ITAM multiplicity (shown in legend), which have been modeled as Gamma distributions with varying scale parameters but all have equivalent total density. The right panel shows the convolution of these two functions.

fig. S5. Representative cytometry data for kinetics of ERK phosphorylation using synthetic receptors

Representative flow cytometry plots of ERK phosphorylation at the indicated time-points after rapalog drug addition (2.5μM) to cell conjugates. Jurkat T cells expressing the synthetic receptors (with number of ITAMs indicated in legend) were conjugated with FRB-expressing Raji B cells for 30 mins prior to rapalog addition, as described in the main text. The plots show the data from one representative experiment, with ERK phosphorylation intensity derived solely from gated cell conjugates gated during flow cytometry.

fig. S6. Supplementary data for the mechanism of ZAP70 activation by autophosphorylation

(**A**) The distribution and expression levels of the constructs transfected in the reconstituted cell system after single-cell sorting, the cells which were used for the TCR triggering kinetic analysis. A negative control using non-transfected HEK cells is shown in each plot (filled gray). For TCR and CD45 surface density, the equivalent expression for Jurkat T cells is also shown (dotted line).

(**B**) Schematic of the standard receptor triggering model, where pMHC binding creates the complex that can be phosphorylated by LCK at each ITAM (only one is shown for clarity). ZAP70 binding leads to Y319 phosphorylation by LCK (red). Phosphorylation of ZAP70 activation loop (Y493) by LCK activates ZAP70 (green), which then drives LAT phosphorylation (blue). Ligand dissociation (k_{off}) was assumed to reset the complex as in the standard kinetic proofreading model.

(**C**) BioNetGen was used to simulate the model in B, with the presence of unmodified complex at t=0 s acting as the initiation for activation. The value of k_{off} was set to 0 so that the effect of ITAM multiplicity could be explored in isolation. The model was simulated with receptors bearing 1-6 ITAMs (colored scale) and the kinetics of LAT phosphorylation by ZAP70 were plotted. The right panel shows the derived reaction rate for this process.

(**D**) Modification of the receptor triggering model in B, which now incorporates autophosphorylation as an essential component of ZAP70 activation. LCK-mediated phosphorylation of ZAP70 at Y493 is still present but at a 100-fold lower rate compared to the standard model above (shown as gray arrow). This initial modification can then drive subsequent ZAP70 activation through *trans*-autophosphorylation (shown as green plus sign), which we assume can only occur within a single receptor and not between receptors.

(**E**) BioNetGen was used to simulate the model in D, with the presence of unmodified complex at t=0 s acting as the initiation for activation. The value of k_{off} was set to 0 so that the effect of ITAM multiplicity could be explored in isolation. The model was simulated with receptors bearing 1-6

ITAMs (colored scale) and the kinetics of LAT phosphorylation by ZAP70 were plotted. The right panel shows the derived reaction rate for this process.

fig. S7. Supplementary data for the CD19 CAR-T cell experiments

(**A**) Schematic of CAR constructs, showing the antibody fragment that recognizes a CD19 epitope along with intracellular sequence of CD3ζ that contains 0-3 ITAMs, using the same point mutations as for the synthetic receptors. The CD3ζ-duplicated CAR variant is also shown. Additional CAR signaling motifs have been removed for clarity.

(**B**) Plots showing the purity of the human $CD4^+$ T cells used in the CAR-T cell assays. Purified T cells were stained with either CD19 and CD8α antibodies as a control, or with CD3 and CD4 antibodies to show purity of > 95 % $CD4^+$ $CD3^+$ cell population.

(**C**) Engineered K562 target cells expressing CD19 at low (red), normal (green) and high (blue) levels are shown, in the context of an isotype control (filled gray) and CD19 expression on the Raji B-cell line (purple).

(**D**) Representative flow cytometry plots of CD137 expression as a function of CAR expression. Human $CD4^+$ T cells expressing the αCD19 CAR were mixed with K562 target cells expressing CD19 for 24 hours, as described in the main text. The plots show the data from one representative experiment. The columns represent the number of ITAMs present on the CAR and the rows define the level of CD19 present on the target cells. T cells were gated from the cell mixture using CD3 staining and CAR^+ T cells were then further gated for analysis using the mRuby2 fluorophore fused to the CAR construct.

(**E**) Human $CD4^+$ T cells expressing the αCD19 CAR with the number of ITAMs shown in legend were activated with K562 target cells expressing the designated level of CD19. Representative

flow cytometry data from one experiment of T-cell activation is shown, measured by CD69 expression, with cells gated for equivalent receptor surface expression. The CD69 expression using the 'High'-expressing target cells was substantially decreased over the other target conditions, which is most likely due to the subsequent downregulation of CD69 after very efficient cell activation.

(**F** and **G**) Data from E were used to calculate the fraction of T cells that had been activated (F) and the mean CD69 intensity of this activated fraction (G) at the CD19 target density shown in the legend. The mean of three independent experiments is shown for each data point, with error bars representing SEM.

Table S1. Oligonucleotide sequences

Sequences of the oligonucleotide primers used in this study.

Note S1. BioNetGen model of proximal TCR signaling

Reaction network written using BioNetGen that models the proximal TCR signaling events, incorporating ZAP70 trans-autophosphorylation as an essential component of the activation pathway.

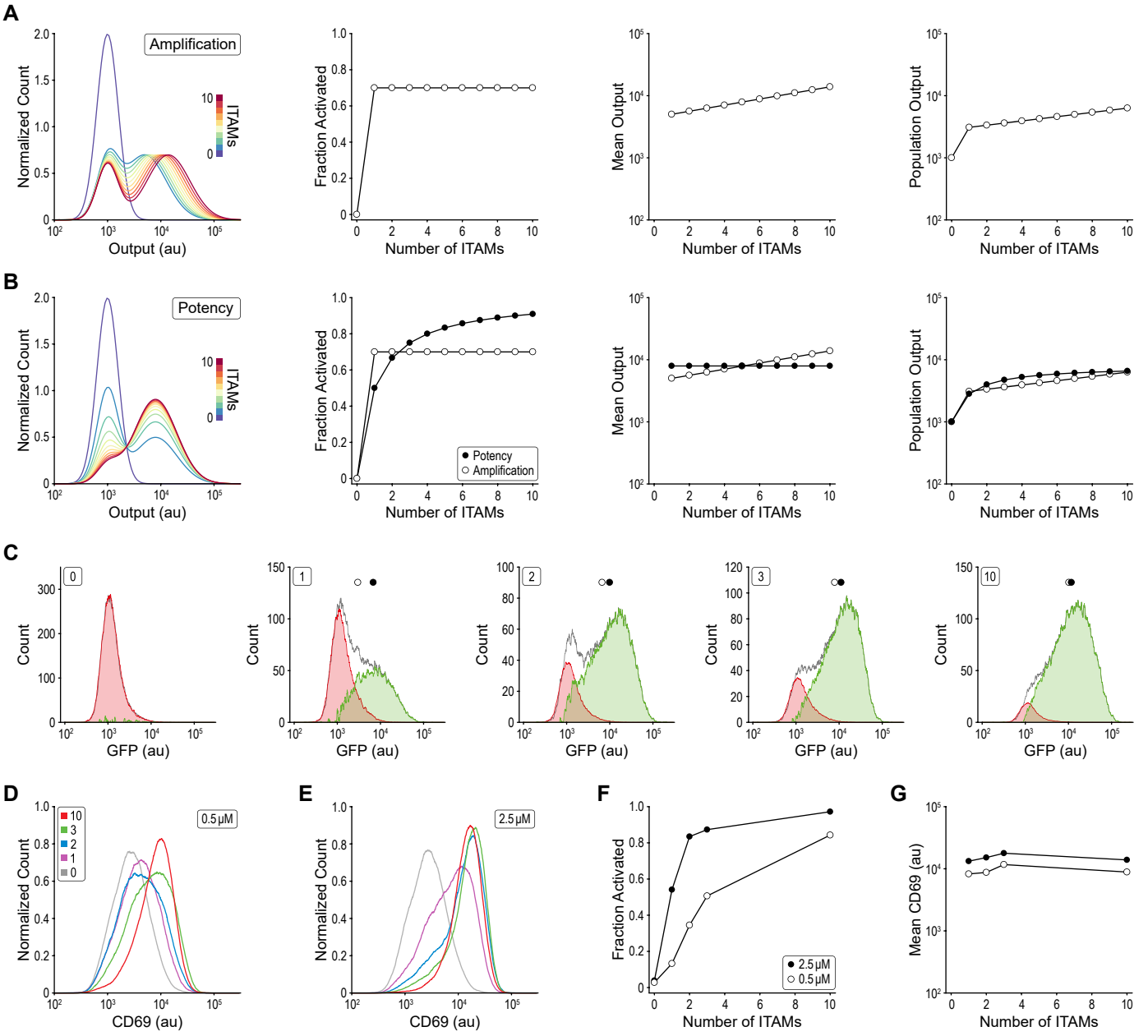

fig. S1. Supplementary data for downstream T-cell activation using synthetic receptors. (**A**) Model data for how signal amplification mediated by ITAM multiplicity might be realized. The first panel shows mock data where successive ITAMs from 1 to 10 (see color legend) increase the signaling output by 12%. This presents as a continuous increase in the signal/noise ratio between the positive and background peaks but not the fraction of activated cells (second panel). The increase in absolute mean output of the activated fraction and the total population is shown in the third and last panels, respectively. (**B**) Model data for how increased receptor potency mediated by ITAM multiplicity might be realized. The first panel shows mock data where successive ITAMs from 1 to 10 (see color legend) increase the fraction of cell that are activated, assumed to be a monotonic function (second panel). This presents as a continuous increase in the ratio between the positive and negative peaks but not the signal/noise. The absolute mean output of the activated fraction and the total population is shown in the third and last panels, respectively. (**C**) Representative examples of how the distribution of activated cells was extracted from the histogram of GFP expression. Data is from the experiment activated using 2.5 μM rapalog with ITAM multiplicity shown in white boxes. The background distribution from Jurkat T cells that had been activated with vehicle control (red area) was used to 'unmix' the histogram, by fitting it under the line through least-squares optimization. This was then subtracted from the total histogram to define the activated or 'positive' distribution (green area). The open circles denote the mean of the total histogram whereas the filled circles show the equivalent mean for the activated distribution. (**D** and **E**) Jurkat T cells expressing the synthetic receptor with number of ITAMs shown in legend were activated with FRB-expressing Raji B cells in the presence of 0.5 μM (D) or 2.5 μM (E) rapalog. Representative flow cytometry data for T cell activation is shown, measured by CD69 expression, with cells gated for equivalent receptor surface expression. (**F** and **G**) Data from D and E were used to calculate the fraction of T cells that had been activated (F) and the mean CD69 intensity of this activated fraction (G) at the rapalog concentration shown in the legend.

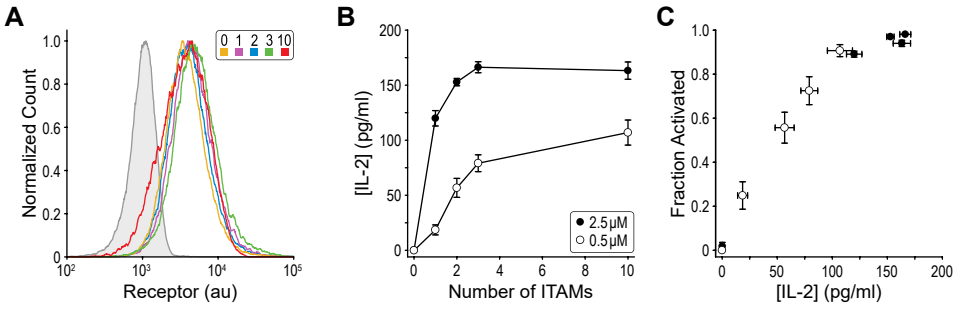

fig. S2. Effect of ITAM multiplicity on IL-2 cytokine secretion. (**A**) Surface expression of the synthetic receptors on T cells used in the IL-2 secretion and phospho-ERK experiments described in the main text, showing that they are essentially equivalent. The number of ITAMs present in each receptor is denoted in the legend. (**B**) Synthetic receptor-expressing T cells were conjugated with ligand-presesnting Raji B cells in the presence of the rapalog drug (concentration shown in legend) and left to activate for 16 hours. The cells were then centrifuged and the supernatant removed for analysis of IL-2 secretion. An ELISA was performed to measure the IL-2 concentration from all samples in technical triplicates, with a known standard used to calibrate absorbance readings to absolute levels of IL-2. The mean of three independent experiments is shown for each data point, with error bars representing SEM. (**C**) The resuspended cell pellet from the same assay was also subjected to flow cytometry analysis to determine the fraction of GFP-positive T cells at the single-cell level. This was then plotted against the measured IL-2 concentration, which demonstrated a strong correlation between the two downstream signaling outputs.

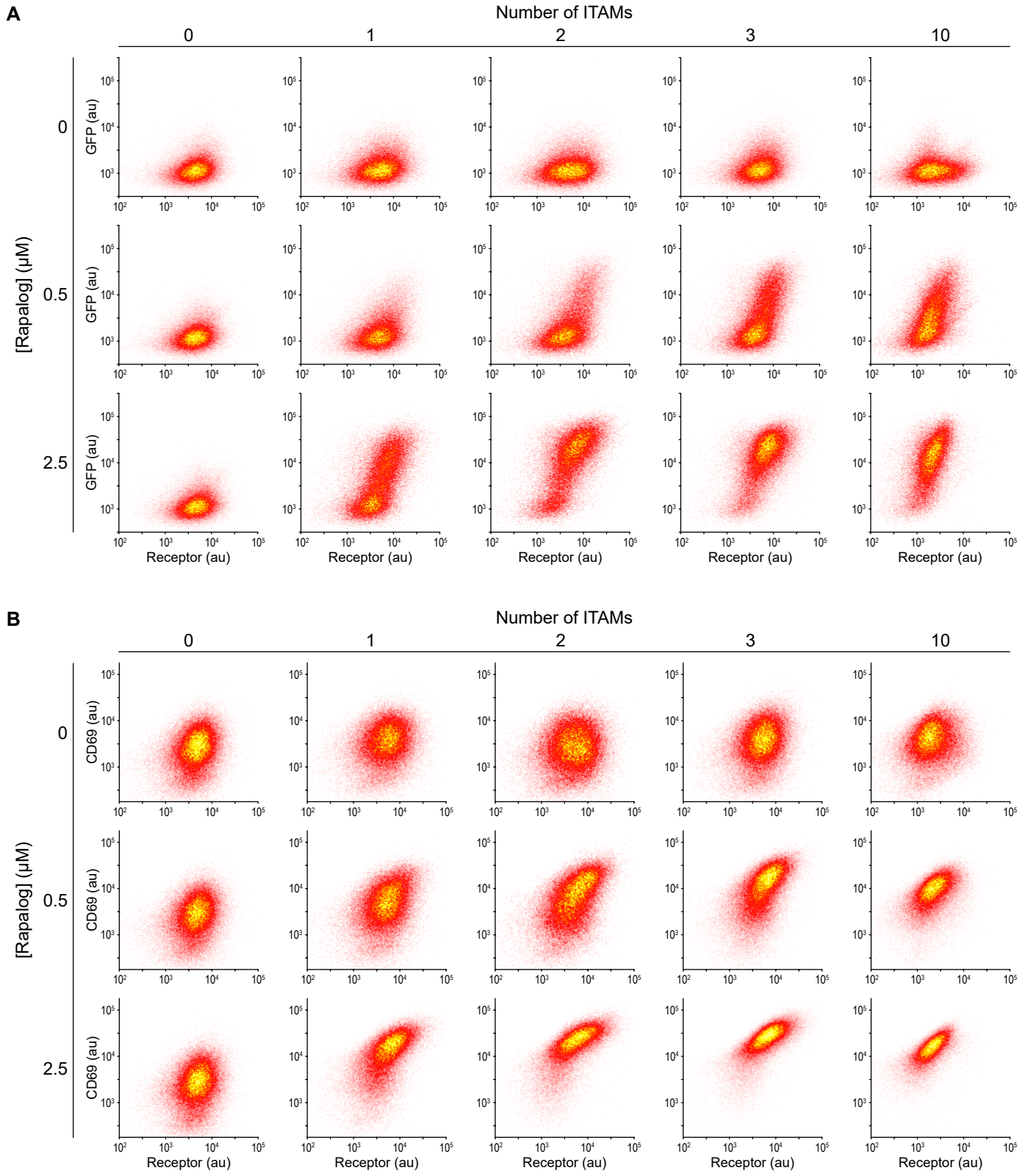

fig. S3. Representative cytometry data for downstream T cell activation using synthetic receptors. (**A** and **B**) Representative flow cytometry plots of NFAT-mediated GFP expression (A) or CD69 expression (B) as a function of synthetic receptor expression. Jurkat T cells expressing the receptors were conjugated with FRB-expressing Raji B cells for 16 hours, as described in the main text. The plots show the data from one representative experiment. The columns represent the number of ITAMs present on the synthetic receptor and the rows define the rapalog concentration used to drive receptor-induced activation.

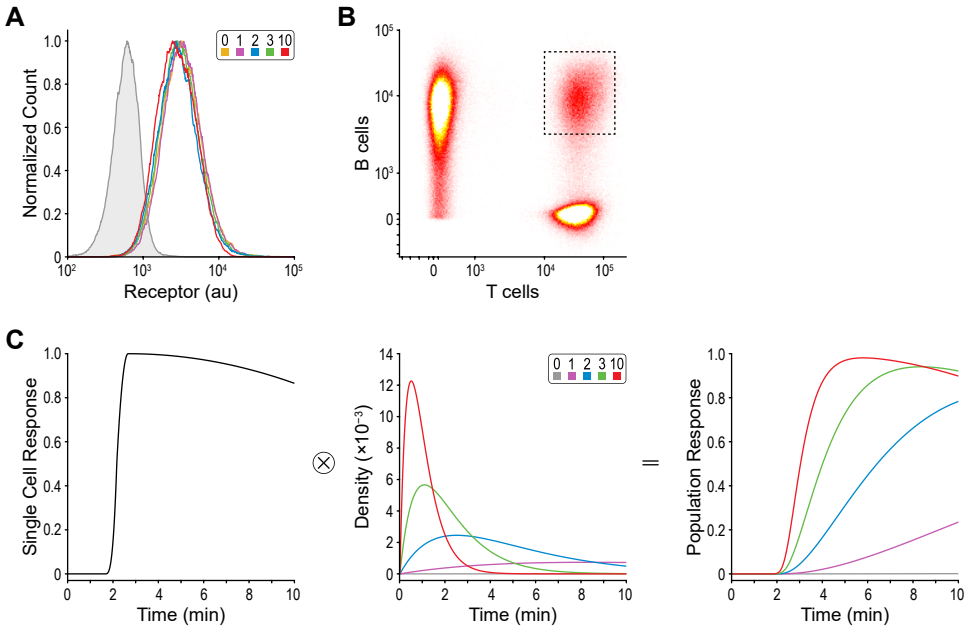

fig. S4. Supplementary data for Ca^{2+} flux data using synthetic receptor. (**A**) Surface expression of the synthetic receptors used in the Ca^{2+} flux experiments described in the main text, showing that they are essentially equivalent. The number of ITAMs present in each receptor is shown in the legend, with the gray histogram showing control staining of untransduced Jurkat T cells.. (**B**) Representative plot of flow cytometry data showing the gating for conjugates formed between iRFP713^{+} Jurkat T cells and mTagBFP^{+} Raji B cells. The boxed area shows the region used to isolate conjugates for the subsequent kinetic analyses. (**C**) Model data to show that the Ca^{2+} flux data presented in the main text can be explained as the convolution of a uniform individual cellular response and a temporal distribution dictated by receptor ITAM multiplicity. The left panel shows an idealized Ca^{2+} flux profile for a single cell (the impulse response), which was constructed from simple piecewise functions. The middle panel shows different temporal distributions of activation to represent different ITAM multiplicity (shown in legend), which have been modeled as Gamma distributions with varying scale parameters but all have equivalent total density. The right panel shows the convolution of these two functions.

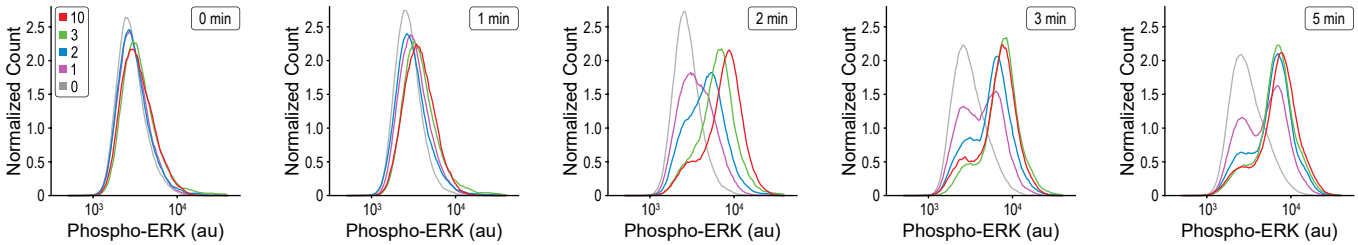

fig. S5. Representative cytometry data for kinetics of ERK phosphorylation using synthetic receptors. Representative flow cytometry plots of ERK phosphorylation at the indicated time-points after rapalog drug addition (2.5 μM) to cell conjugates. Jurkat T cells expressing the synthetic receptors (with number of ITAMs indicated in legend) were conjugated with FRB-expressing Raji B cells for 30 mins prior to rapalog addition, as described in the main text. The plots show the data from one representative experiment, with ERK phosphorylation intensity derived solely from gated cell conjugates gated during flow cytometry.

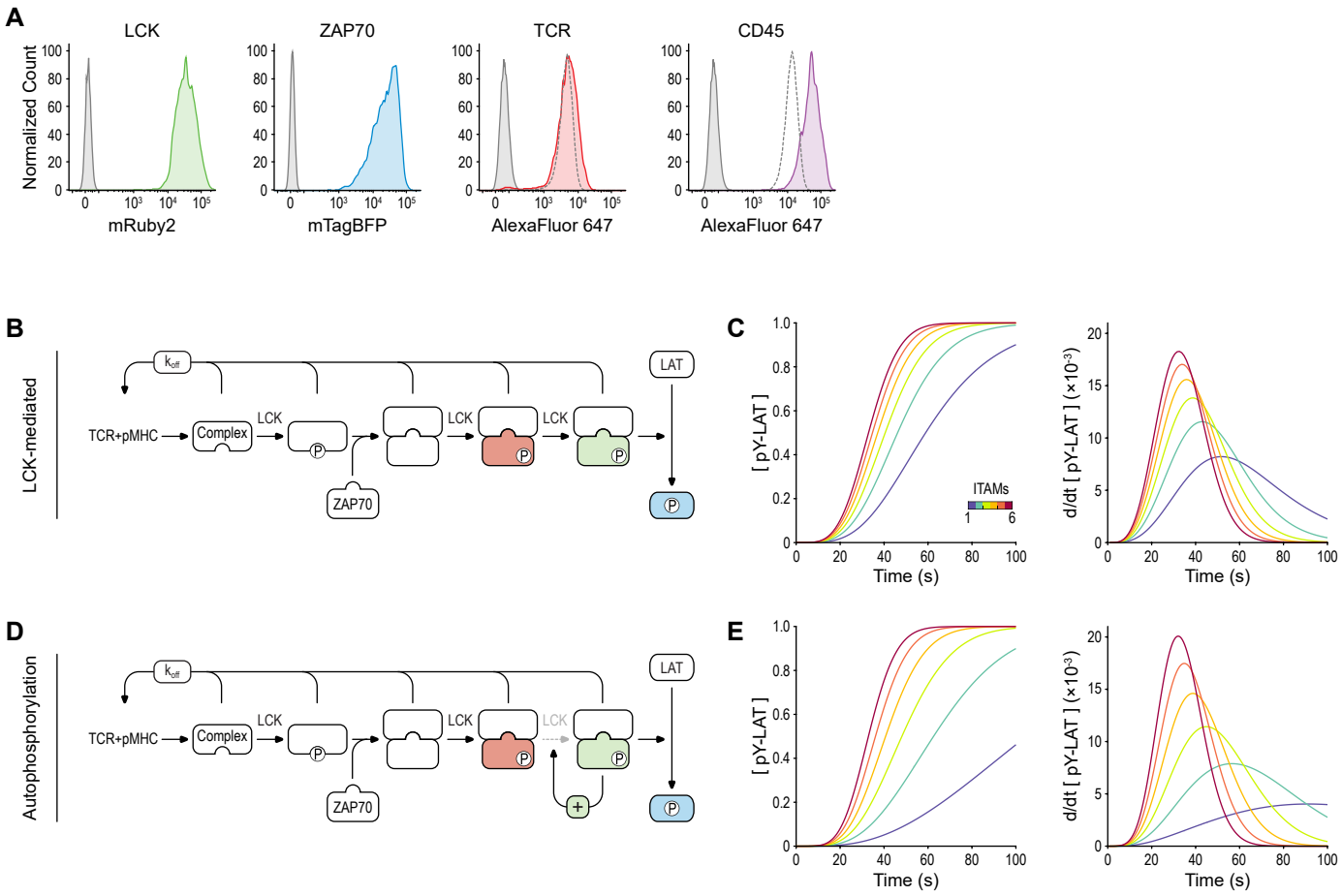

fig. S6. Supplementary data for the mechanism of ZAP70 activation by autophosphorylation. (**A**) The distribution and expression levels of the constructs transfected in the reconstituted cell system after single-cell sorting, the cells which were used for the TCR triggering kinetic analysis. A negative control using non-transfected HEK cells is shown in each plot (filled gray). For TCR and CD45 surface density, the equivalent expression for Jurkat T cells is also shown (dotted line). (**B**) Schematic of the standard receptor triggering model, where pMHC binding creates the complex that can be phosphorylated by LCK at each ITAM (only one is shown for clarity). ZAP70 binding leads to Y319 phosphorylation by LCK (red). Phosphorylation of ZAP70 activation loop (Y493) by LCK activates ZAP70 (green), which then drives LAT phosphorylation (blue). Ligand dissociation (k_{off}) was assumed to reset the complex as in the standard kinetic proofreading model. (**C**) BioNetGen was used to simulate the model in B, with the presence of unmodified complex at t=0 s acting as the initiation for activation. The value of k_{off} was set to 0 so that the effect of ITAM multiplicity could be explored in isolation. The model was simulated with receptors bearing 1-6 ITAMs (colored scale) and the kinetics of LAT phosphorylation by ZAP70 were plotted. The right panel shows the derived reaction rate for this process. (**D**) Modification of the receptor triggering model in B, which now incorporates autophosphorylation as an essential component of ZAP70 activation. LCK-mediated phosphorylation of ZAP70 at Y493 is still present but at a 100-fold lower rate compared to the standard model above (shown as gray arrow). This initial modification can then drive subsequent ZAP70 activation through trans-autophosphorylation (shown as green plus sign), which we assume can only occur within a single receptor and not between receptors. (**E**) BioNetGen was used to simulate the model in D, with the presence of unmodified complex at t=0 s acting as the initiation for activation. The value of k_{off} was set to 0 so that the effect of ITAM multiplicity could be explored in isolation. The model was simulated with receptors bearing 1-6 ITAMs (colored scale) and the kinetics of LAT phosphorylation by ZAP70 were plotted. The right panel shows the derived reaction rate for this process.

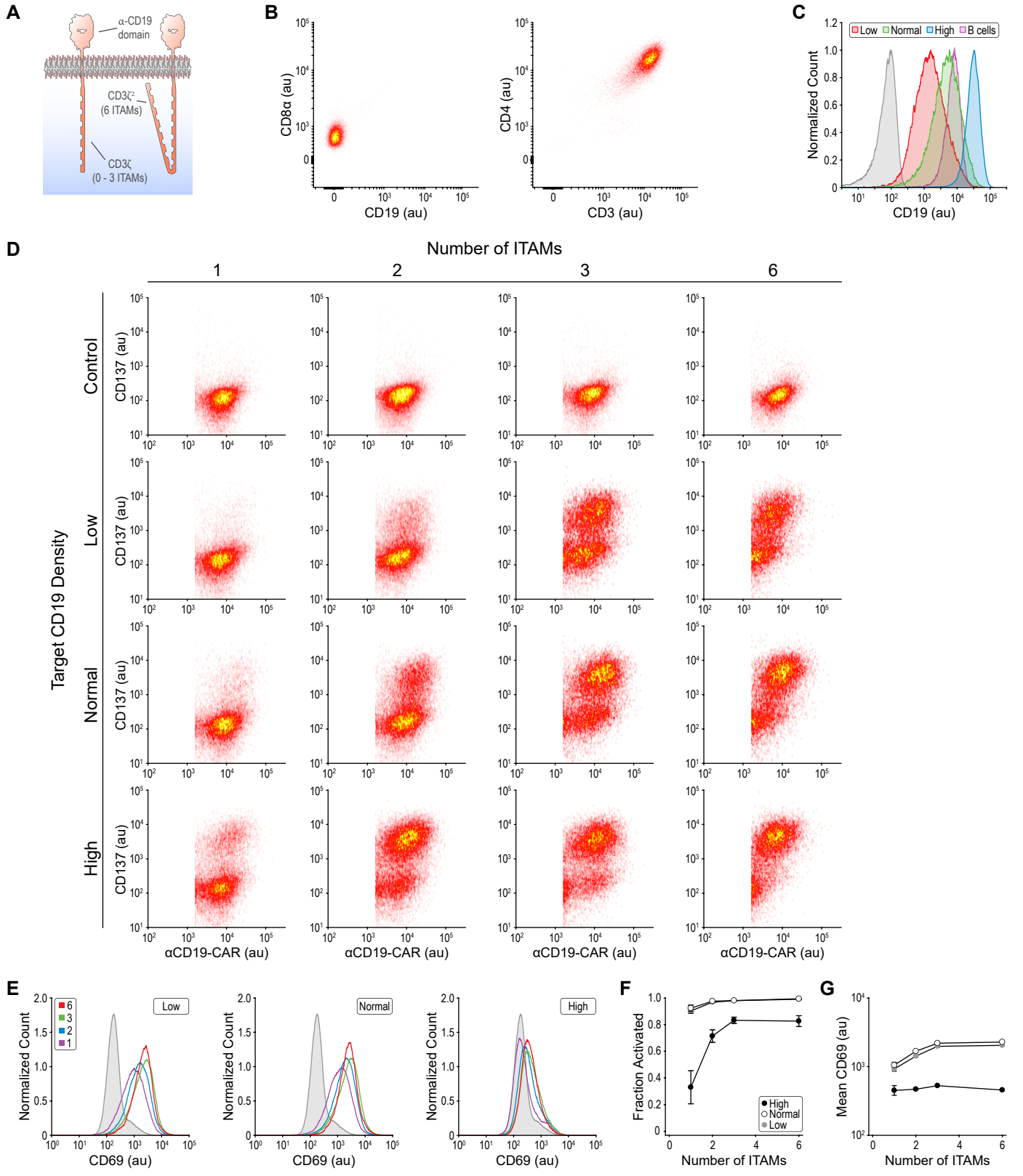

fig. S7. Supplementary data for the CD19 CAR T cell experiments. (**A**) Schematic of CAR constructs, showing the antibody fragment that recognizes a CD19 epitope along with intracellular sequence of CD3ζ that contains 0-3 ITAMs, using the same point mutations as for the synthetic receptors. The CD3ζ-duplicated CAR variant is also shown. Additional CAR signaling motifs have been removed for clarity. (**B**) Plots showing the purity of the human CD4⁺ T cells used in the CAR T cell assays. Purified T cells were stained with either CD19 and CD8α antibodies as a control, or with CD3 and CD4 antibodies to show purity of > 95 % CD4⁺ CD3⁺ cell population. (**C**) Engineered K562 target cells expressing CD19 at low (red), normal (green) and high (blue) levels are shown, in the context of an isotype control (filled gray) and CD19 expression on the Raji B-cell line (purple). (**D**) Representative flow cytometry plots of CD137 expression as a function of CAR expression. Human CD4⁺ T cells expressing the αCD19 CAR were mixed with K562 target cells expressing CD19 for 24 hours, as described in the main text. The plots show the data from one representative experiment. The columns represent the number of ITAMs present on the CAR and the rows define the level of CD19 present on the target cells. T cells were gated from the cell mixture using CD3 staining and CAR⁺ T cells were then further gated for analysis using the mRuby2 fluorophore fused to the CAR construct. (**E**) Human CD4⁺ T cells expressing the αCD19 CAR with the number of ITAMs shown in legend were activated with K562 target cells expressing the designated level of CD19. Representative flow cytometry data from one experiment of T cell activation is shown, measured by CD69 expression, with cells gated for equivalent receptor surface expression. The CD69 expression using the 'High'-expressing target cells was substantially decreased over the other target conditions, which is most likely due to the subsequent downregulation of CD69 after very efficient cell activation. (**F** and **G**) Data from E were used to calculate the fraction of T cells that had been activated (F) and the mean CD69 intensity of this activated fraction (G) at the CD19 target density shown in the legend. The mean of three independent experiments is shown for each data point, with error bars representing SEM.

Supplementary Methods

Key Resources Table

REAGENT or RESOURCE	SOURCE	IDENTIFIER
Antibodies		
Rabbit polyclonal anti-human ZAP70 (Y493)	Cell Signaling Technology	Cat#: 2704
Rabbit polyclonal anti-human ZAP70	Cell Signaling Technology	Cat#: 3165
Rabbit polyclonal anti-human LAT (pY132)	Thermo Fisher Scientific	Cat#: 44-224
Rabbit polyclonal anti-human LAT	Cell Signaling Technology	Cat#: 9166
Goat polyclonal anti-rabbit IgG (DyLight-800)	Cell Signaling Technology	Cat#: 5151
Mouse anti-human CD86 (Alexa Fluor-647)	Biolegend	Cat#: 305416
Mouse anti HA-Tag (Alexa Fluor-647)	Cell Signaling Technology	Cat#: 3444
Mouse anti-human CD69 (Brilliant Violet 605)	Biolegend	Cat#: 310937
Human TruStain FcX (FcR blocking)	Biolegend	Cat#: 422302
Mouse anti-human CD19 (Alexa Fluor 647)	Biolegend	Cat#: 302220
Mouse phospho-ERK1/2 (Alexa Fluor 488)	Cell Signaling Technology	Cat#: 4374
Mouse anti-human CD137 (Brilliant Violet 421)	Biolegend	Cat#: 309820
Mouse anti-human CD19 (clone FMC63)	Absolute Antibody	Cat#: Ab00613-2.0
Biological Samples		
Healthy human whole blood	Cambridge Blood Biobank	N/A
Chemicals, Peptides, and Recombinant Proteins		
A/C Heterodimerizer (AP21967)	TaKaRa Clontech	Cat#: 635057
Indo-1 LR (AM)	TEFLab	Cat#: TEF0145
Pluronic F-127	Sigma-Aldrich	Cat#: P2443
ImmunoCult CD3/CD28/CD2 T Cell Activator	StemCell Technologies	Cat#: 10970
Lenti-X Concentrator	TaKaRa Clontech	Cat#: 631231
Recombinant Protein L (Biotinylated)	Thermo Fisher Scientific	Cat#: 29997
Streptavidin (Alexa Fluor 488)	Biolegend	Cat#: 405235
Critical Commercial Assays		
EasySep Direct Human CD4 Isolation Kit	StemCell Technologies	Cat#: 19662
Quantum Alexa Fluor 647 MESF Beads	Bangs Laboratories	Cat#: 647
IL-2 Human Uncoated ELISA Kit	Thermo Fisher Scientific	Cat#: 88-7025-22

Experimental Models: Cell Lines		
HEK-293T: Human adherent cell-line	ATCC	Cat#: CRL-11268
Jurkat: Human T-cell leukemia cell-line	A. Weiss (UCSF)	N/A
Raji: Human B-cell lymphoma cell-line	ATCC	Cat#: CCL-86
K562: Human CML cell-line	ATCC	Cat#: CCL-243
Recombinant DNA		
pCMVΔR8.91	(Zufferey et al., 1997)	N/A
pMD2. G	Gift from Didier Trono	Addgene#: 12259
pHR-CD3	(James and Vale, 2012)	N/A
pHREF-1G4	This study	N/A
pHREF-LCK-mRuby2	This study	N/A
pHR-ZAP70-mTagBFP	This study	N/A
pHR-LAT	(James and Vale, 2012)	N/A
pHR-CBP/CSK-mIFP	This study	N/A
pHCM-CD45RO-mEGFP	This study	N/A
pHR-HA:FKBP-CD86-CD3ζ	This study	N/A
pHR-HA:FKBP-TCRα	This study	N/A
pHR-CD19^{TM} (and pHRSV-/pHREF-)	This study	N/A
pHREF-CAR-mRuby2 (αCD19)	This study	N/A
pcDNA3-mRuby2	(Lam et al., 2012)	Addgene#: 40260
mIFP-N1	(Yu et al., 2014)	Addgene#: 54620
Sequence-Based Reagents		
For all primers sequences, see Table S1	This study	N/A
Software and Algorithms		
FIJI (ImageJ): Image analysis	Schindelin et al., 2012	https://fiji.sc/
MATLAB R2015b: Data processing	MathWorks	N/A
FlowJo V10.2: Data processing	FlowJo	N/A
Excel 2013: Data processing	Microsoft	N/A
BioNetGen: Simulations	Faeder et al., 2009	http://bionetgen.org
Illustrator CC: Figure production	Adobe	N/A

Methods Details

Cell culture

All cell lines were maintained at 37°C with 5% CO_2 in a fully-humidified incubator. The adherent human cell-line HEK-293T (HEK) and all derivatives were grown in DMEM (Sigma-Aldrich) supplemented with 10% FBS (Life Technologies) and antibiotics. Wildtype Jurkat T cells and Raji B cells (including all derivatives thereof) were grown in RPMI-1640 (Sigma-Aldrich), supplemented with 10% FBS, 10mM HEPES and antibiotics. The K562 cell-line and CD19-expressing variants were grown in IMDM (Life Technologies) supplemented with 10% FBS. Human primary $CD4^+$ T cells were purified by negative selection using the EasySep Direct Human CD4 Isolation kit (StemCell Technologies) following the manufacturer's protocol, which gave a >98% $CD4^+$ population. Primary cells were grown in ImmunoCult-XF T Cell Expansion Medium (StemCell Technologies).

Vector Construction

All oligonucleotides used in this study are given in Table S1. In cases where the amplified gene had a required restriction site already present, the codon sequence was conservatively mutated by site-directed mutagenesis. For simplified cloning, the pHR backbone was modified to the general scheme:

EcoRI–[**Promoter**]–*MluI*–[**Gene**]–*BamHI*–[**xFP**]–Stop–*NotI*

For the two-gene constructs, this was converted to:

EcoRI–[**Promoter**]–*AsiSI*–[**Gene1**]–*SpeI*–**P2A**–*MluI*–[**Gene2**]–*BamHI*–[**xFP**]-Stop–*NotI*

P2A denotes the self-cleaving 2A protein sequence from Porcine Teschovirus-1 and xFP denotes an unspecified fluorescent protein. For all vectors, PCR products were digested and ligated into the required lentiviral vector backbone, then transformed into DH5α chemically-competent *E.*coli and spread on antibiotic-resistant agar plates. After PCR was used to confirm gene insertion and orientation, a single colony was used to inoculate LB media containing the appropriate antibiotic. A DNA miniprep of this liquid culture was performed using the PureLink kit (Life Technologies). The integrity of all amplified DNA sequences and point mutations were confirmed by sequencing. Where point mutations were made, overlapping extension PCR was used for site-directed mutagenesis. To expand the expression range of a particular construct, the standard SFFV promoter

in the pHR-SIN lentiviral backbone was replaced with different promoters that drive a range of expression levels (mHSP < ΔSV40 < EF1α < SFFV < CMV), giving rise to the pHRI, pHRSV, pHREF, pHR and pHCM vectors. respectively.

pHREF-1G4 : 1G4α and 1G4β sequences were amplified and inserted as Gene1 and Gene2, respectively, into pHR vector using primers *1-4* and pHR-1G4αβεζ template (James and Vale, 2012). The EF1α promoter was amplified from a pEF6 vector using primers *5+6*.

pHREF-LCK-mRuby2 : The mRuby2 fluorophore was amplified using primers *7+8* and inserted in pHR-LCK (James and Vale, 2012). The EF1α promoter was then amplified using primers *5+9* and replaced the SFFV promoter.

pHR-ZAP70-mTagBFP : The fluorophore from pHR-pMHC-mTagBFP was excised and inserted into pHR-ZAP70 (James and Vale, 2012).

pHR-CBP/CSK-mIFP : The genes for CBP and CSK were amplified from pHR-CBP and pHR-CSK using primers *10+11* and *12+13*, respectively (James and Vale, 2012). The PCR products were inserted as Gene1 and Gene2 into the bicistronic vector, and then the fluorophore mIFP was amplified from mIFP-N1 using primers *14+15* and fused to the C-terminus of CSK.

pHCM-CD45RO-mEGFP : The gene for CD45RO (including a N-terminal His tag) was amplified from a published construct (James et al., 2011) using primers *16+17*. The SFFV promoter was replaced with the CMV equivalent using primers *18+19*. To drive high expression, the SV40 introns (16S) were synthesized as a GeneArt String, amplified using primers *20+21* and inserted as BssHII/MluI fragment at the 5'-end of CD45RO gene. Finally, the mEGFP fluorophore was fused to the C-terminus of CD45.

pHR-FKBP-CD86-CD3ζ : The construct is based on $FKBP^{Ex}\zeta^{Int}$ described previously (James and Vale, 2012). The signal peptide of CD86 was replaced with one from Gaussia luciferase and included an HA-epitope at the mature N-terminus to allow surface quantification. To facilitate the mutation of the CD3ζ ITAMs, a SpeI restriction site was inserted just after CD86 by overlapping extension PCR with primers *22-25*.

pHR-FKBP-TCRα : The FKBP domain was fused to the mature N-terminal sequence of the Jurkat TCRα chain by extension PCR, using primers *22*,*26-28*. The sequences of FKBP-CD86-CD3ζ and a gene-synthesized fragment of Jurkat TCRα were used as the templates.

pHR-CD19^{TM} : The sequence of human CD19 (without intracellular sequence) was synthesized as a GeneArt String and amplified using primers *29+30* and inserted into the pHR vector backbone. To modulate the surface expression of the protein, the SFFV promoter was replaced with the EF1α promoter from pHREF-LCK-mRuby2 or the ΔSV40 promoter from pHRSV-CD86-FKBP, creating pHREF-CD19^{TM} and pHRSV-CD19^{TM}, respectively.

pHREF-CAR-mRuby2 (αCD19) : The sequence of the αCD19 antibody fragment from clone FMC63, along with CD8 stalk and TM regions and 4-1BB intracellular domain were amplified from a synthesized GeneArt String using primers *31+32*. This PCR product was inserted as a MluI/SpeI fragment into pHR-FKBP-CD86-CD3ζ, which fused the CAR to the CD3ζ chain, along with the different ITAM variants. The fluorophore mRuby2 was fused to the C-terminus and the EF1α promoter was inserted in the vector to replace the SFFV version. To make the 6 ITAM variant, a synthesized GeneArt String was designed with a second copy of the CD3ζ ITAMs synonymously mutated, amplified using primers *33+34* and inserted into the vector as a SpeI/BamHI fragment.

Lentivirus production

HEK cells were distributed into 6-well plates to give 60-80% confluency at the point of transient transfection. GeneJuice (EMD Millipore) was used according to the manufacturer's instructions to transfect 1.5 μg total DNA into each well, using the lentiviral backbone vector (derived from pHRSIN-CSGW), pCMVΔ8.91 (encoding essential packaging genes) and pMD2.G (encoding VSV-G gene to pseudotype virus) at a 2:2:1 ratio. After 48-72 hours, the supernatant from each well was removed, centrifuged at 14,000×*g* for 2 minutes to remove debris and then incubated with ~1 x 10^6 target cells for 16 hr. Fresh medium was then added and the cells were recovered for at least 3 days until expression of the target protein could be detected. The expression level of the transduced gene was monitored regularly and fresh cells were prepared if expression decreased significantly.

Flow Cytometry

Cell samples to be analyzed by flow cytometry were pipetted into standard tubes and centrifuged at 800×*g* for 3 minutes, with pellets flick-resuspended. Where required, primary antibodies were used at a working concentration of ~10 μg/ml, diluted in Flow wash buffer [2.5% (v/v) FBS, 0.1% (w/v) NaN_3 in PBS, pH 7.4] and incubated on ice for at least 30 min, with regular agitation. For Raji B cells, endogenous Fc receptors were pre-blocked with Human TruStain FcX for 10 minutes at room temperature. Samples were washed with 3 ml Flow wash buffer and centrifuged as before. When the primary antibody was fluorescently conjugated, the pellet was resuspended and fixed in Flow fix buffer [1.6% (v/v) formaldehyde, 2% (w/v) glucose, 0.1% (w/v) NaN_3 in PBS, pH 7.4). When a secondary labeled-antibody was required, an equivalent staining protocol was used, with the antibody at 20 μg/ml, prior to washing and fixing. The flow cytometer was set up to ensure the most appropriate dynamic range between the negative and positive controls for each fluorescence channel and at least 30,000 gated cells were collected for each analysis.

Chemically-inducible receptor system

Construction of the vectors for the FKBP-CD86-CD3ζ synthetic receptor (previously described as $FKBP^{Ex}\zeta^{Int}$), its ligand, FRB^{Ex}, and the Raji cell-line expressing this ligand have been previously described (James and Vale, 2012), although the receptor now included an HA-epitope at the mature N-terminus for quantification of expression. FKBP is the FKBP12 domain harboring the F36V mutation and the FRB domain has the T2098L mutation, which permits use of the 'rapalog' series of dimerizing drugs. To decrease the number of ITAMs within this construct, we used overlap extension PCR to mutate the first Tyr in each ITAM to Phe, starting from the C-terminal ITAM. Permuting the ITAM mutation had no effect on the observed response, confirming the distributive nature of ITAM phosphorylation (data not shown). To engineer a receptor complex with 10 ITAMs, we fused FKBP to the mature N-terminus of the TCRα sequence from Jurkat T cells (along with an HA-epitope), which was incorporated into the endogenous Jurkat TCR complex through competition with the native TCRα gene product.

A lentiviral construct was designed that expressed GFP under the control of NFAT-response elements, which also constitutively expressed iRFP713 from a separate promoter. The latter cassette allowed the cells to be easily separated from a mixture. A clonal Jurkat derivative was created that expressed this construct (J.NFAT) and expressed GFP under TCR stimulation (data not shown).

The synthetic receptors were transduced into J.NFAT cells and expression was measured using the HA-epitope, which could be quantified using fluorescent beads as described above.

Calcium flux analysis

For each experiment, ~5×10^5 J.NFAT cells expressing the required orthogonal receptor were loaded with 5μg/ml Indo-1, a fluorescent Ca^{2+} indicator, and 0.1% Pluronic F-127 in serum-free medium at 37°C for 30 minutes. Labeled cells were washed in PBS and resuspended in residual medium, which was ~50μl. Raji-FRB^{Ex} cells (~5×10^5) were also pelleted and resuspended similarly. To a PCR strip-tube, 50μl of each cell line was added and the cells were allowed to sediment under gravity at 37°C, which caused very efficient cell conjugation without centrifugation. After this incubation, conjugates were gently resuspended and added to cytometry tube with 500μl complete medium. Prior to use, conjugates were 'rested' at room temperature for at least 15 minutes, as we found that a temperature differential can cause Jurkat cells to spontaneously flux Ca^{2+} to a limited extent. Conjugates were analyzed at room temperature on an LSRFortessa flow cytometer (equipped with a UV laser; BD) for 30 seconds to acquire a baseline Indo-1 reading before AP21967 (A/C) Heterodimerizer was added at required concentration and the Indo-1 ratio was followed for ~10 minutes, or until the sample was exhausted.

The cytometry data was gated in FlowJo, first on live cells (by forward/side scatter) and then on conjugated cells using a Raji (mTagBFP, with Indo-1 compensated from channel) *vs* Jurkat (iRFP) plot to identify double-positive events. The gated cells were exported to Matlab for further analysis. For each sample, the data was binned into 1 second windows. The histogram of the Indo-1 ratio at each time-point was calculated prior to normalization using the 2-norm of the vector. The resulting array was either directly plotted to visualize the individual sample or used for further analysis. To separate the background from the fluxing cells, a two-peak Gaussian model was fitted to each time bin to identify the background signal distribution, and a value 2σ from the mean was used as the threshold, which is delineated in the main figure. The median of the Indo-1 ratio above this threshold was calculated for each time-point and, after subtracting the baseline value, is the data presented in the main figure. For each concentration of drug and receptor ITAM variant, the experiment was performed three times, and the mean of these median values is presented, along with a bounding area describing the standard error of the mean at each time-point. For clarity, the

data points have been three-fold decimated in the actual figures, and the bounding area and fit use a moving-average filter to remove high-frequency noise.

Phospho-ERK analysis

For each experiment, ~5×10^5 J.NFAT cells expressing the required synthetic receptor were conjugated with Raji-FRB^{Ex} cells (~1.5×10^6) in an equivalent manner as for the calcium flux assay. in the absence of the rapalog. After 30 minutes at 37°C, cell conjugates were gently resuspended by pipetting. Prior to the initiation of receptor triggering, a sample was taken to define the 0 min time-point. After this, the rapalog drug (AP21967 (A/C) Heterodimerizer) was added at a final concentration of 2.5μM and cells incubated at 37°C. After the required time, 100μl of cell suspension was removed and immediately fixed in 500μl 4% formaldehyde at 37°C for 10 minutes. Cells were then kept on ice prior to washing with 3ml Flow wash buffer. The resuspended pellet was then vortexed while 500μl Perm buffer III (BD Biosciences) cooled to -20°C was added dropwise. After this, samples were left on ice for 30 minutes and then washed twice with 3ml Flow wash buffer. The resuspended pellet was then incubated with the phospho-ERK1/2 (Thr202/Tyr204) Mouse mAb that was directly conjugated with Alexa Fluor 488 (Cell Signaling Technologies) for 45 minutes at room temperature, with regular agitation. After this, stained cells were washed with 3ml Flow wash buffer and fixed with 500μl Flow fix buffer. Samples were then acquired on a flow cytometer as described above.

Despite methanol fixation, the fluorescence from the iRFP713+ JNFAT cells and BFP+ Raji B cells was still readily detectable, allowing us to gate exclusively on cell conjugates for the subsequent analysis of phospho-ERK signal and this is the data presented in the figures of the main text.

Downstream cellular activation

J.NFAT cells expressing the appropriate orthogonal receptor were conjugated to Raji-FRB^{Ex} cells for 30 minutes as described for the calcium flux analysis, except that the cells were conjugated in medium that included the AP21967 (A/C) Heterodimerizer at prescribed concentration. After this incubation, conjugates were transferred to a 24-well plate (1ml/well) under standard culture conditions for 16 hours to allow activation-induced expression of GFP from the NFAT-responsive promoter. Cells were stained with a fluorescently-conjugated antibody against the HA-epitope prior to running the sample on a flow cytometer to measure the receptor expression and GFP expression. Quantification beads that had known amounts of Alexa Fluor-647 were also run to

convert the relative fluorescence of the HA staining to absolute receptors/cell, using the manufacturer-provided value of mean fluorophores per antibody (~5.0). For the CD69 expression data, cells were also labeled with a fluorescently-conjugated anti-CD69 antibody.

The cytometry data was gated in FlowJo, first on live cells (by forward/side scatter) and then on single J.NFAT cells by iRFP713+,mTagBFP- gating. The gated cells were exported to Matlab for further analysis. To calculate the fraction of activated cells and the corresponding mean output response, the data was first gated for equivalent receptor expression and a histogram of this subset was formed. The control sample without drug addition was used to define the background intensity distribution, which was used to 'unmix' the positive population from the sample histogram. To do this, a Matlab script was used to fit the left-hand side of the background distribution to the sample histogram using least-squares regression. Subtraction of this background population from the histogram then created the sample distribution of the activated T cells. The fraction of activated cells was calculated as the area of the positive over the total distribution and the arithmetic mean of the log-transformed data was calculated for the activated distribution.

For the derivation of receptor potency, the control sample without drug addition was used to define a threshold based on 99% of GFP intensity, so that expression above this was deemed an activated cell. The expression of the synthetic receptor was used to bin the data, and the fraction of activated cells in each bin was calculated. For all datasets, experiments were performed three times, and the mean of these independent tests is presented in the main figure, along with a bounding area describing the standard error of the mean at each bin. Datasets were also fitted using a 3-parameter logistic regression, with the asymptote constrained to that of the 3 ITAMs data. The EC_{50} values shown in the main figure were derived from these fits.

Detection of IL2 cytokine production

An equivalent protocol was used as for the downstream cellular activation assay to drive IL2 cytokine production. The only significant difference was that the synthetic receptor-expressing cells were sorted to give similar surface expression since it would not be possible to correlate receptor density with IL2 production. After 16 hours, the supernatant from activated cells (1ml/well of a 24-well plate) was removed from each well. The concentration of IL2 in the supernatant was then quantified using the IL-2 Human ELISA Kit (Thermo Fisher Scientific) according to the manufacturer's instructions. When required, samples were diluted to ensure that the absorbance

values at 450 nm were in the linear range of the IL2 standard curve. The IL2 concentrations reported in the text were interpolated from the standard curve, using the IL2 standard provided in the kit.

To correlate IL2 production with downstream activation, the cell pellets remaining after supernatant removal were subjected to flow cytometry for NFAT-mediated GFP expression using an equivalent approach as described in the downstream cellular activation section.

Cellular reconstitution of TCR triggering kinetics

We used lentiviral transduction and single-cell sorting to create a clonal HEK cell derivative that expressed the 1G4 TCR complex at physiological surface expression (fig. S4A). These cells were distributed into 6-well plates to give 40-60% confluency at the point of transient transfection. GeneJuice was used according to the manufacturer's instructions to transfect 2 µg total DNA into each well, consisting of constructs encoding LCK-mRuby2, ZAP70-mTagBFP, LAT, CBP/CSK-mIFP and CD45RO-mEGFP (at a ratio of 1:1:1:1:2). Transfected cells were trypsinized two days after transfection and sorted by flow cytometry, gating on all expressed fluorophores to give a near-homogeneous population of transfected cells (fig. S4A). Typically, we sorted an entire 6-well plate to give ~5×10^5 positive cells, resuspended in complete medium at ~400 cells/µl. After taking an aliquot of these cells as a baseline control, 100µM pervanadate was mixed with the cells and 50µl aliquots were removed every 7.5 seconds into pre-frozen tubes held in a metal rack, maintained at -80˚C using dry ice. Pervanadate was freshly prepared by mixing 0.25% H_2O_2 with 17mM sodium orthovanadate (final concentrations) prior to dilution to 1mM with water after two minutes.

Frozen samples were then overlaid with 2× lysis buffer [2% Nonidet P40, 2mM orthovanadate, 2mM PMSF, Complete inhibitor cocktail (EDTA-free) in Tris-buffered saline (TBS)] and allowed to thaw on wet ice for at least one hour. Lysed samples were centrifuged at 20,000×*g* for 10 minutes to remove nuclear material and then heat-denatured in 4× LDS sample buffer (Life Technologies) including DTT at 70˚C for 10 minutes. Samples were loaded over two NuPAGE 4-12% Bis-Tris 26-well protein gels (Life Technologies) and run in MOPS buffer at 200V for 55 minutes. Gels were then blotted onto nitrocellulose (0.2µm pore-size) using the iBlot (Life Technologies) system (P0; 8min), cut into two strips corresponding to the molecular weight range for ZAP70 and LAT, respectively, and blocked with 2.5% skimmed milk powder (Sigma-Aldrich) in TBS. The blots were then incubated with the required primary antibody in block buffer that

included 0.1% Tween-20 (milk/TBS-T) overnight at 4˚C, washed four times in milk/TBS-T buffer before incubating with a fluorescent secondary antibody (described in the Resource Table) for 1 hour at room temperature. Blots were finally washed in TBS-T four times and then left in TBS. An Odyssey CLx Infrared Imaging System (Li-Cor) was used to image the stained blots using the following settings: auto-intensity in 800nm channel; 84μm resolution.

A custom Fiji plugin was used to extract the integrated intensities of the appropriate bands, which were corrected for local background fluorescence. To convert the raw intensities derived from the blots into absolute numbers so that different experiments could be directly compared, a subset of samples at equivalent time-points were run on a single gel and the integrated band intensities for both the phosphorylated (I_P) and native proteins (I_N) were calculated. The fraction of phosphorylated protein (I_P / I_N) at the time-point was then used to scale the raw data to that value. All experiments were performed at least three times, and the mean of these scaled data series is presented in the main text, along with a bounding area describing the standard error of the mean at each time-point. Datasets were fitted in Matlab using a 5-parameter logistic regression.

Modelling the proximal TCR signaling network

BioNetGen (Faeder et al., 2009) was used to model TCR triggering, incorporating the known inititating steps in TCR triggering, leading to LAT phosphorylation. The network was used to model the reaction starting from complex formation and evolve the kinetics of receptor triggering in the absence of ligand dissocation, to study the effect of ITAM multiplicity in isolation. An example of the reaction network for the system with 3 ITAMs is shown in Note S1. The two Tyr residues of an ITAM were modeled as a single phosphorylation event to minimise complexity. To define all the TCR-bound ZAP70 variants with different number of ITAM binding sites, a simple bash script was used to iterate over all potential combinations. Because BioNetGen does not account for multiple enzymes being bound to a single species (in this case, multiple ZAP70 bound to the TCR), it was necessary to include rules that explicitly accounted for this when describing LAT phosphorylation by ZAP70. Up to 6 ZAP70-binding sites could be computed (over ~20 hours) but more than this became unfeasible. For the model without ZAP70 auto-phosphorylation, the rate parameters were simply adjusted to 'linearise' ZAP70 activation. Mass action kinetics, rather than Michaelis-Menten, were used to simplify the reaction network and reduce computational complexity.

Chimeric antigen receptor activation

The chimeric antigen receptor (CAR) targeted to CD19 described in the paper was gene-synthesized (GeneArt, ThermoFisher) and inserted to a lentiviral vector. The C-terminus of the construct was fused to the mRuby2 fluorophore for detection of transduced cells. Mutation of the ITAMs of the CD3ζ present in the construct was performed as described for the orthogonal receptor above. To construct a CAR variant with 6 ITAMs, the CD3ζ intracellular sequence was duplicated, and all synonymous mutations in one half were made. This sequence was synthesized and inserted into the CAR vector. To construct target cells expressing different levels of the CD19 protein, the CD19 gene was inserted into lentiviral vectors with different promoters that drive a range of expression levels (mHSP < ΔSV40 < EF1α < SFFV). K562 cells were transduced with these constructs and, when needed, cells were sorted on CD19 expression to provide the three cell lines described in the main text. Fc receptor blocking was used to remove non-specific binding of the antibodies. Raji B cells were used as a positive control to show the expected level of CD19 on 'normal' B cells.

Frozen stocks of human primary $CD4^+$ T cells were thawed for 2 hours in complete medium prior to activation using a CD3/CD28/CD2 T-Cell Activator to drive their proliferation. During this period, lentivirus was produced for the CAR constructs and concentrated ~40× using the Lenti-X reagent. After 48 hours of activation, ~1.5×10^5 primary T cells in 50µl were incubated with ~150µl viral supernatant overnight under normal growth conditions. CAR expression was confirmed by labeling with biotinylated Protein L at 20µg/ml in PBS after extensive washing in PBS, which should recognize the antibody fragment expressed by the CAR. This binding was then detected by fluorescently-labeled streptavidin (at 5µg/ml), which correlated strongly with mRuby2 fluorophore intensity also present in the CAR construct. Transduced cells were left to proliferate over ~10 days until there was a clear decrease in cell volume, judged by scatter on a flow cytometer. T cells were then conjugated with K562 target cells equivalently to that for the J.NFAT cells. When required, the target cells were pre-incubated with 20µg/ml anti-CD19 antibody (clone FMC63) on ice for 30 minutes to block the CAR epitope, and the antibody was present throughout the subsequent incubations. After 24 hours, cells were stained with fluorescently-labeled antibodies against CD137 (BV421), CD69 (AF488) and CD3 (AF647) and were then measured by flow cytometry.

The cytometry data was gated in FlowJo, on live cells (by forward/side scatter), then CD3+ to select the T-cell population. Finally, this subset was gated on mRuby2 expression to only include CAR-expressing T cells in the analysis (~20 - 30%). As all CAR variants expressed at approximately equivalent levels, no receptor binning was needed and the activated fraction of cells and mean output response were calculated equivalently as for synthetic receptors, described above. CD137 and CD69 expression were both used as a readout of T-cell activation. For all datasets, experiments were performed three times, and the mean of these independent tests is presented in the main figure, along with error bars describing the standard error of the mean.

Table S1

Gene	Oligo#	Sequence (5'-3')	Restriction
1G4α	1	TAGTAGCGATCGCACCATGGAGACCCTCTTGGGCCTGC	AsiSI
	2	CTACTAACTAGTGCTGGACCACAGCCGCAGCGTC	SpeI
1G4β	3	TAGTAGACGCGTATGAGCATCGGCCTCCTGTG	MluI
	4	CTACTAGCGGCCGCTCAAGGATCCTTTCTCTTGACCATGGCCATC	BamHI/NotI
EF1α Pr	5	TAGTAGGAATTCGCTAGCTAGGTCTTGAAAG	EcoRI
	6	CTACTAGCGATCGCCCTGTGTTCTGGCGGCAAACC	AsiSI
mRuby2	7	TAGTAGGGATCCACCGGTCGCCACCATGGTGTCTAAGGGCGAAGAGC	BamHI
	8	CTACTAGCGGCCGCTCACTTGTACAGCTCGTCCATCCC	NotI
EF1α Pr	9	CTACTAACGCGTCCTGTGTTCTGGCGGCAAACC	MluI
CBP	10	TAGTAGCGATCGCCACCATGGGGCCCGCGGG	AsiSI
	11	CTACTAACTAGTCAGCCTGGTAATATCTCTGCCTTGC	SpeI
CSK	12	TAGTAGACGCGTATGTCAGCAATACAGGCCGC	MluI
	13	CTACTAGCGGCCGCTCATGGATCCAGGTGCAGCTCGTGGGTTTTG	Bam/NotI
mIFP	14	TAGTAGGGATCCACCGGTCGCCACCATG	BamHI
	15	CTACTAGCGGCCGCTCATTTGGACTGAGACTGTGCAAAGC	NotI
CD45RO	16	TAGTAGACGCGTGCCACCATGGGCATCCTTCCCAGCCCTGGGATGCCTGC	MluI
	17	CTACTAGCGGCCGCTCAAGGATCCGAACCTTGATTTAAAGCTGGACTTG	Bam/NotI
CMV Pr	18	TAGTAGGAATTCTAGTTATTAATAGTAATCAATTACGG	EcoRI
	19	CTACTAACGCGTGACAATTCTCGAGAGCTCCAGATCTGAGTC	MluI
SV40Intron	20	TAGTAGTAGGCGCGCTCAGATCG	-
	21	CTACTACTAACGCGTAGCTTTTAGAGC	-
SP:HA	22	TAGTAGACGCGTGCCACCATGGGAGTCAAAGTTCTGTTTGCCC	MluI
CD3ζ	23	CTACTAGGATCCCGAGGGGGCAGGGCC	BamHI
	24	GAAGAAGAAGCGGCCTCGGACTAGTGCAGACGCCCCCGCGTACCAG	-
	25	CTGGTACGCGGGGGCGTCTGCACTAGTCCGAGGCCGCTTCTTCTTC	-
FKBP-TCRα	26	GAAGCGGAGGTAGTGGTGGAAGCCAGTCGGTGACCCAGCTTGGCAG	-
	27	CTGCCAAGCTGGGTCACCGACTGGCTTCCACCACTACCTCCGCTTC	-
	28	CTACTAGCGGCCGCTCAGCTGGACCACAGCCGCAGCGTC	NotI
CD19™	29	TAGTAGACGCGTGCCACCATGCCACCTCCTCGCCTCC	MluI
	30	CTACTAGCGGCCGCTCAAGGATCCGTCATTCGCTTTCTTTTCCTCCTCAG	Bam/NotI
CD19 CAR	31	TAGTAGACGCGTGCCACCATGGCCTTACCAGTGACCGCC	MluI
	32	CTACTAACTAGTCCTGCTGAACTTCACTCTCAGTTC	SpeI
CD3ζ[2]	33	TAGTAGACTAGTGCAGACGCCCCCGCGTACCAG	SpeI
	34	CTACTAGCGGCCGCTCAAGGATCCCTTGGAGGGAGAGCCTGCATATGC	Bam/NotI

Note S1

```
#BioNetGen code for simplified TCR triggering network, invoking auto-phosphorylation in ZAP70 activation
begin parameters
#Kinase catalysis rates
  lck_cat                                                                                    0.1
  lckW_cat                                                                                   0.001
  zapP_cat                                                                                   1
  zapL_cat                                                                                   0.1
#Binding parameters, ZAP70 binding is irreversible for simplicity
  zap_on                                                                                     0.001
  koff                                                                                       0
#Total protein concentrations
  TCR_T                                                                                      1
  LCK_T                                                                                      2
  ZAP70_T                                                                                    100
  LAT_T                                                                                      1
end parameters
saveParameters()

begin molecule types
  #TCR denotes the TCR/pMHC complex for convenience
  #For all, ~P corresponds to the phosphorylated state
  TCR(I1~U~P,I2~U~P,I3~U~P)
  LCK()
  ZAP70(b,St~U~P~T)
  #St~P corresponds to pY319 and St~T to pY319+pY493
  LAT(St~U~P)
  Null()
  #Null is a placeholder for the dissociated TCR complex
end molecule types

begin seed species
  TCR(I1~U,I2~U,I3~U)                                                                        TCR_T
  LCK()                                                                                      LCK_T
  ZAP70(b,St~U)                                                                              ZAP70_T
  LAT(St~U)                                                                                  LAT_T
end seed species

begin reaction rules
  #Lck phosphorylating the TCR
  LCK() + TCR(I1~U) -> LCK() + TCR(I1~P)                                                     lck_cat
  LCK() + TCR(I2~U) -> LCK() + TCR(I2~P)                                                     lck_cat
  LCK() + TCR(I3~U) -> LCK() + TCR(I3~P)                                                     lck_cat
...
```

```
  #ZAP70 binding to the TCR
  ZAP70(b,St~U) + TCR(I1~P) -> ZAP70(b!1,St~U).TCR(I1~P!1)                                                    zap_on
  ZAP70(b,St~U) + TCR(I2~P) -> ZAP70(b!1,St~U).TCR(I2~P!1)                                                    zap_on
  ZAP70(b,St~U) + TCR(I3~P) -> ZAP70(b!1,St~U).TCR(I3~P!1)                                                    zap_on

  #Lck phosphorylation of ZAP70 at Y319
  LCK() + ZAP70(b!1,St~U).TCR(I1~P!1) -> LCK() + ZAP70(b!1,St~P).TCR(I1~P!1)                                  lck_cat
  LCK() + ZAP70(b!1,St~U).TCR(I2~P!1) -> LCK() + ZAP70(b!1,St~P).TCR(I2~P!1)                                  lck_cat
  LCK() + ZAP70(b!1,St~U).TCR(I3~P!1) -> LCK() + ZAP70(b!1,St~P).TCR(I3~P!1)                                  lck_cat

  #LCK phosphorylating ZAP70 at Y493 to become activated
  LCK() + ZAP70(b!+,St~P) -> LCK() + ZAP70(b!+,St~T)                                                          lckW_cat

  #ZAP70 transphosphorylation at Y493 to become activated
  #ITAM 1 paired with 2
  ZAP70(b!1,St~T).ZAP70(b!2,St~P).TCR(I1~P!1,I2~P!2)-> ZAP70(b!1,St~T).ZAP70(b!2,St~T).TCR(I1~P!1,I2~P!2)   zapP_cat
  ZAP70(b!1,St~P).ZAP70(b!2,St~T).TCR(I1~P!1,I2~P!2)-> ZAP70(b!1,St~T).ZAP70(b!2,St~T).TCR(I1~P!1,I2~P!2)   zapP_cat

  #ITAM 1 paired with 3
  ZAP70(b!1,St~T).ZAP70(b!2,St~P).TCR(I1~P!1,I3~P!2)-> ZAP70(b!1,St~T).ZAP70(b!2,St~T).TCR(I1~P!1,I3~P!2)   zapP_cat
  ZAP70(b!1,St~P).ZAP70(b!2,St~T).TCR(I1~P!1,I3~P!2)-> ZAP70(b!1,St~T).ZAP70(b!2,St~T).TCR(I1~P!1,I3~P!2)   zapP_cat

  #ITAM 2 paired with 3
  ZAP70(b!1,St~T).ZAP70(b!2,St~P).TCR(I2~P!1,I3~P!2)-> ZAP70(b!1,St~T).ZAP70(b!2,St~T).TCR(I2~P!1,I3~P!2)   zapP_cat
  ZAP70(b!1,St~P).ZAP70(b!2,St~T).TCR(I2~P!1,I3~P!2)-> ZAP70(b!1,St~T).ZAP70(b!2,St~T).TCR(I2~P!1,I3~P!2)   zapP_cat

  #ZAP70 phosphorylating LAT
  #Phosphorylation of LAT by TCR bound with 1 ZAP70
  ZAP70(b!1,St~T).TCR(I1~P!1) + LAT(St~U) -> ZAP70(b!1,St~T).TCR(I1~P!1) + LAT(St~P) zapL_cat …
exclude_reactants(1,ZAP70(b!1,St~T).TCR(I2~P!1),ZAP70(b!1,St~T).TCR(I3~P!1))
  ZAP70(b!1,St~T).TCR(I2~P!1) + LAT(St~U) -> ZAP70(b!1,St~T).TCR(I2~P!1) + LAT(St~P) zapL_cat …
exclude_reactants(1,ZAP70(b!1,St~T).TCR(I1~P!1),ZAP70(b!1,St~T).TCR(I3~P!1))
  ZAP70(b!1,St~T).TCR(I3~P!1) + LAT(St~U) -> ZAP70(b!1,St~T).TCR(I3~P!1) + LAT(St~P) zapL_cat …
exclude_reactants(1,ZAP70(b!1,St~T).TCR(I1~P!1),ZAP70(b!1,St~T).TCR(I2~P!1))
  #Phosphorylation of LAT by TCR bound with 2 ZAP70
  ZAP70(b!1,St~T).ZAP70(b!2,St~T).TCR(I1~P!1,I2~P!2) + LAT(St~U) -> ZAP70(b!1,St~T).ZAP70(b!2,St~T).TCR(I1~P!1,I2~P!2)
… + LAT(St~P) 2*zapL_cat exclude_reactants(1,ZAP70(b!1,St~T).TCR(I3~P!1))
  ZAP70(b!1,St~T).ZAP70(b!2,St~T).TCR(I1~P!1,I3~P!2) + LAT(St~U) -> ZAP70(b!1,St~T).ZAP70(b!2,St~T).TCR(I1~P!1,I3~P!2)
… + LAT(St~P) 2*zapL_cat exclude_reactants(1,ZAP70(b!1,St~T).TCR(I2~P!1))
  ZAP70(b!1,St~T).ZAP70(b!2,St~T).TCR(I2~P!1,I3~P!2) + LAT(St~U) -> ZAP70(b!1,St~T).ZAP70(b!2,St~T).TCR(I2~P!1,I3~P!2)
… + LAT(St~P) 2*zapL_cat exclude_reactants(1,ZAP70(b!1,St~T).TCR(I1~P!1))
  #Phosphorylation of LAT by TCR bound with 3 ZAP70
  ZAP70(b!1,St~T).ZAP70(b!2,St~T).ZAP70(b!3,St~T).TCR(I1~P!1,I2~P!2,I3~P!3) + LAT(St~U) -> …
ZAP70(b!1,St~T).ZAP70(b!2,St~T).ZAP70(b!3,St~T).TCR(I1~P!1,I2~P!2,I3~P!3) + LAT(St~P) 3*zapL_cat
```

```
  #TCR complex dissociation
  TCR() -> Null()                                                                    koff
end reaction rules

begin observables
  Molecules ZAPpY319        ZAP70(b!+,St~P)  ZAP70(b!+,St~T)
  Molecules pLAT            LAT(St~P)
end observables

saveConcentrations()
generate_network({overwrite=>1})
saveParameters()
simulate({suffix=>"withFB",method=>"ode",t_end=>100,n_steps=>200})
resetParameters()
resetConcentrations()
setParameter("lckW_cat",0.1)
setParameter("zapP_cat",0)
saveParameters()
simulate({suffix=>"noFB",method=>"ode",t_end=>100,n_steps=>200})
```